iScience

CellPress
OPEN ACCESS

Article

Bifidobacterium affects antitumor efficacy of oncolytic adenovirus in a mouse model of melanoma

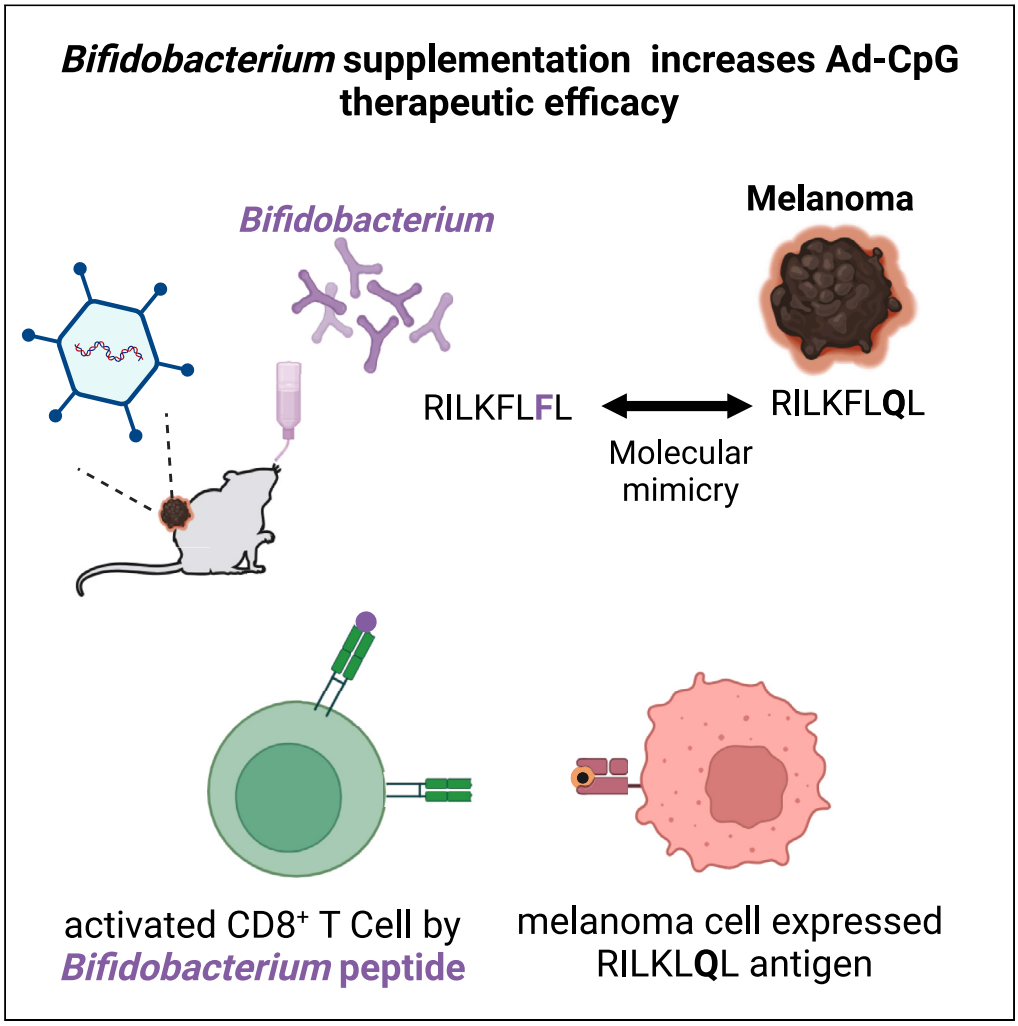

Lorella Tripodi, Sara Feola, Ilaria Granata, ..., Barbara Szomolay, Vincenzo Cerullo, Lucio Pastore

vincenzo.cerullo@helsinki.fi (V.C.)
lucio.pastore@unina.it (L.P.)

Highlights

Therapeutic antitumor efficacy of Ad-CpG is gut microbiota mediated

Bifidobacterium supplementation increases the antitumoral efficacy of Ad-CpG s *in vivo*

Enrichment of species belonging to Firmicutes in the microbiota of Ad-CpG-treated mice

Immunogenicity of a Bifidobacterium peptide, highly similar to a melanoma peptide

Tripodi et al., iScience *26*, 107668
October 20, 2023
https://doi.org/10.1016/j.isci.2023.107668

iScience

CellPress
OPEN ACCESS

Article

Bifidobacterium affects antitumor efficacy of oncolytic adenovirus in a mouse model of melanoma

Lorella Tripodi,[1,2] Sara Feola,[3] Ilaria Granata,[4] Thomas Whalley,[5] Margherita Passariello,[1,2] Cristian Capasso,[3] Ludovica Coluccino,[1,2] Maria Vitale,[1] Giulia Scalia,[1] Laura Gentile,[1] Claudia De Lorenzo,[1,2] Mario Rosario Guarracino,[6] Giuseppe Castaldo,[1,2] Valeria D'Argenio,[1,7] Barbara Szomolay,[8] Vincenzo Cerullo,[2,3,*] and Lucio Pastore[1,2,9,*]

SUMMARY

Gut microbiota plays a key role in modulating responses to cancer immunotherapy in melanoma patients. Oncolytic viruses (OVs) represent emerging tools in cancer therapy, inducing a potent immunogenic cancer cell death (ICD) and recruiting immune cells in tumors, poorly infiltrated by T cells. We investigated whether the antitumoral activity of oncolytic adenovirus Ad5D24-CpG (Ad-CpG) was gut microbiota-mediated in a syngeneic mouse model of melanoma and observed that ICD was weakened by vancomycin-mediated perturbation of gut microbiota. Ad-CpG efficacy was increased by oral supplementation with Bifidobacterium, reducing melanoma progression and tumor-infiltrating regulatory T cells. Fecal microbiota was enriched in bacterial species belonging to the Firmicutes phylum in mice treated with both Bifidobacterium and Ad-CpG; furthermore, our data suggest that molecular mimicry between melanoma and Bifidobacterium-derived epitopes may favor activation of cross-reactive T cells and constitutes one of the mechanisms by which gut microbiota modulates OVs response.

INTRODUCTION

In the era of incredible successes achieved by immunotherapy, many efforts are focusing on the identification of the sources of the variability of therapies, observed in clinical outcomes.[1,2] The basis for variable patients' responses to antibodies targeting programmed cell death protein 1 (PD-1) and cytotoxic T lymphocyte antigen-4 (CTLA-4/B7.1/B7.2) involves many biological factors, including genetic variability, differences in tumor mutational loads, and microbiota composition. The role of gut microbiota in the modulation of response to antitumoral therapies is becoming evident even considering new studies on its impact on the response to both chemotherapy[3] and immunotherapy.[4,5] In addition, tumor growth is modulated by intestinal microbiota: in fact, bacterial depletion by aggressive antibiotic treatment induces faster tumor progression and reduces the efficacy of many treatments, as shown in murine model of breast and colorectal cancer.[6,7] Multiple studies show that microbiota plays a pivotal role in modulating response to immune-checkpoint inhibitors (ICIs) in mice models and patients, promoting its ability to affect treatment outcomes.[8,9] Strong evidence in support of the immunomodulatory activity exerted by the gut microbiota was confirmed by the loss of therapeutic activity of recombinant monoclonal antibody anti-CTLA-4 (9D9) against sarcoma in mice housed under specific pathogen-free (SPF) conditions and then treated with multiple broad-spectrum antibiotics to sterilize the gut.[10] Sivan et al. demonstrated that members of the Bifidobacteriales were abundant in mice that exhibited reduced growth of melanomas and improved cytotoxic T lymphocytes (CTLs)-mediated immunosurveillance. Supplementation with *Bifidobacterium breve* or *Bifidobacterium longum* into Bifidobacteriales-free mice was sufficient to reduce melanoma growth and restore anti-melanoma CTL response.[11] Several studies indicate that gut microbiota affects the efficacy of cancer immunotherapies by engaging innate and/or adaptive immune systems[9,12–14]; for instance, commensal bacterium *Bifidobacterium breve* stimulates antitumoral immune responses by amplifying specific T cells; the latter cross-react with model neoantigen expressed in melanoma tumor.[15–17] Indeed, specific antigens, derived from peptides of intracellular

[1]CEINGE Biotecnologie Avanzate Franco Salvatore s.c.a.r.l, Napoli, Italy
[2]Dipartimento di Medicina Molecolare e Biotecnologie Mediche, Università degli Studi di Napoli Federico II, Napoli, Italy
[3]Drug Research Program (DRP), ImmunoViroTherapy Lab (IVT), Division of Pharmaceutical Biosciences, Faculty of Pharmacy, University of Helsinki, Viikinkaari 5E, 00790 Helsinki, Finland
[4]Institute for High-Performance Computing and Networking National Research Council Branch of Naples, 509066 Naples, Naples, Italy
[5]School of Biosciences, Cardiff University, Cardiff CF10 3AX, Wales, UK
[6]University of Cassino and Southern Lazio Department of Economics and Law, 154984 Cassino, Frosinone, Italy
[7]Department of Human Sciences and Quality of Life Promotion, San Raffaele Open University, Rome, Italy
[8]Division of Infection and Immunity and Systems Immunity Research Institute, Cardiff University School of Medicine, Cardiff CF14 4XN, Wales, UK
[9]Lead contact
*Correspondence: vincenzo.cerullo@helsinki.fi (V.C.), lucio.pastore@unina.it (L.P.)
https://doi.org/10.1016/j.isci.2023.107668

bacteria peptides, can be presented within human leukocyte antigen (HLA)-I and HLA-II molecules expressed on the surface of melanoma cells and elicit a tumor-infiltrating T cell immune response. In particular, bacterial peptides that invade cancer cells can be presented on the tumor cell surface and recognized by the immune system.[18] The intratumoral bacteria repertoire identified in melanoma patients can affect T cell immune reactivity in the tumor microenvironment (TME).[19] All these discoveries consistently support the idea that the gut microbiota plays a pivotal role in shaping antitumoral immune responses elicited by several immunotherapies, even if, different scenarios have been identified according to the type of tumor and therapy.[20]

Oncolytic virotherapy is a promising approach in cancer immunotherapy: working as an active immunizing agent, oncolytic viruses (OVs) convert immunologically "cold" tumors into "hot" ones. OVs are very attractive for potential synergistic combination with ICIs; indeed, their ability to recruit CTLs can be combined with the ICIs' skill to avoid tumor immune evasion and therefore induce a sustained response.[21–23] The immune-mediated eradication of tumors through oncolytic adenoviruses makes them a promising strategy for combination therapy[21,24–26] to address the limitations of ICIs. Actually, multiple ongoing clinical trials are aiming to investigate the combined therapeutic efficacy of ICIs and oncolytic adenoviruses.[27] Despite the fact that the role of the gut microbiota in modulating immunotherapy efficacy has been widely considered in many types of cancers, its role in the oncolytic virotherapy of solid tumors has never been investigated to date. Given that gut microbiota influences ICIs efficacy, it is possible to hypothesize that it could also affect the antitumoral activity of oncolytic adenoviruses. In addition, the eligibility of OVs as a valuable candidate for combination therapy with ICIs, whose activity is gut microbiome mediated, is relevant to elucidate the possible role of microbiota in the modulation of response to OV treatment. Here, we decided to investigate whether the efficacy of oncolytic adenovirus Ad5D24-CpG (Ad-CpG) treatment[24] could be affected by the gut microbiota, in a syngeneic mouse model of melanoma. Ad-CpG is a modified version of the oncolytic adenovirus Ad5D24 virus that includes the insertion of 18 immuno-stimulatory CpG islands.[24] We observed that gut microbiota depletion by treatment with antibiotics[10] impaired the response of subcutaneous tumors to Ad-CpG therapy, reducing tumor-infiltrating interferon (IFN)-γ CD8 (cluster of differentiation 8) T cells, confirming the role of intestinal bacteria in the antitumoral responses elicited by Ad-CpG. Considering the ability of *Bifidobacterium* to improve the effector function of tumor-specific $CD8^+$ T cells,[11] we evaluated tumor progression in the same model of melanoma after treatment with a combination of Ad-CpG and *Bifidobacterium* spp. cocktail (Bifidus), used as single agents or in combination, and we observed a reduced tumor progression in mice treated with the combination therapy. To better understand the mechanism responsible for this synergistic effect,[28] we identified all *Bifidobacterium*-derived peptides highly similar to murine melanoma epitopes and evaluated their possible contribution to the antitumoral effect.

RESULTS

Gut microbiota affects the response to Ad-CpG in a syngeneic mouse model of melanoma

The observation that cancer immunotherapy with CTLA-4 and PD-L1 blockade is affected by gut microbiota composition[10,11] prompted us to investigate whether oncolytic virotherapy efficacy could also be influenced by intestinal bacteria. At first, we planned to evaluate whether gut microbiota depletion and unbalance after long-term antibiotic use could affect the response to Ad-CpG therapy. To this end, we treated a group of mice with vancomycin starting two weeks before B16.OVA melanoma cells inoculation until the first intratumoral administration of Ad-CpG, as indicated in the experimental design (Figure 1, panel A). The group of mice treated with vancomycin and Ad-CpG had significantly faster tumor growth compared to the group treated with Ad-CpG alone (Figure 1, panel B); interestingly, tumor progression in the group treated with a combined regimen (Ad-CpG + vancomycin) was comparable to what was observed in mice treated with vancomycin alone. Therefore, vancomycin treatment seems to abrogate the effect of virotherapy. The Ad-CpG-treated tumors showed significantly slower growth kinetics as represented by the area under the curve (AUC) analysis (Figure 1, panel C). Furthermore, the reduced response observed in mice treated with Ad-CpG combined with vancomycin can be better appreciated considering the single tumor growth curves for each mouse treated (20% responders, Figure 1, panel D). Vancomycin treatment however reduced tumor growth compared to mock-treated mice: this observation is consistent with the current literature.[29] To assess how vancomycin pre-treatment influences the immune response induced by Ad-CpG, we analyzed the phenotype of tumor-infiltrating lymphocytes (TILs) in treated mice and controls. Both $CD4^+$ and $CD8^+$ T cells levels were unaffected by vancomycin pre-treatment (Figure 1, panels E and F); on the other hand, the percentage of IFN-γ-producing $CD8^+$ T cells was significantly lower in mice that received the combined regimen compared to mice treated only with Ad-CpG (Figure 1, panel G). The quadrant gating strategy that has been used for all samples is reported in supplemental data (Figure S1). These data suggest that antibiotic pre-treatment causes a reduction of the IFN-γ-secreting $CD8^+$ T cells infiltrating the tumor, negatively affecting the anticancer Ad-CpG efficacy.

Restoring gut microbiota balance reverses the effect of vancomycin treatment on the efficacy of Ad-CpG treatment

In order to confirm that the reduced efficacy of Ad-CpG was due to gut microbiota alterations, we cohoused a group of mice treated with a combined regimen (Ad-CpG + vancomycin) with mice treated with Ad-CpG, as indicated in the experimental design (Figure 2, panel A). We compared melanoma growth in the cohoused group to mice treated with Ad-CpG alone and to an additional group, treated with the same combined regimen but kept isolated. We observed that cohousing significantly reduces differences in tumor growth between mice treated with a combined regimen and those treated with Ad-CpG alone, indicating that a positive perturbation and likely a restoration of gut microbiota occurred (Figure 2, panel B). In addition, tumors of mice treated with the combined regimen and cohoused showed significantly slower growth kinetics compared to the isolated mice as represented by the AUC analysis (Figure 2, panel C). In fact, 100% of responders to Ad-CpG therapy was observed in the cohoused mice treated with the combined regimen while 67% of responders was observed in control group kept

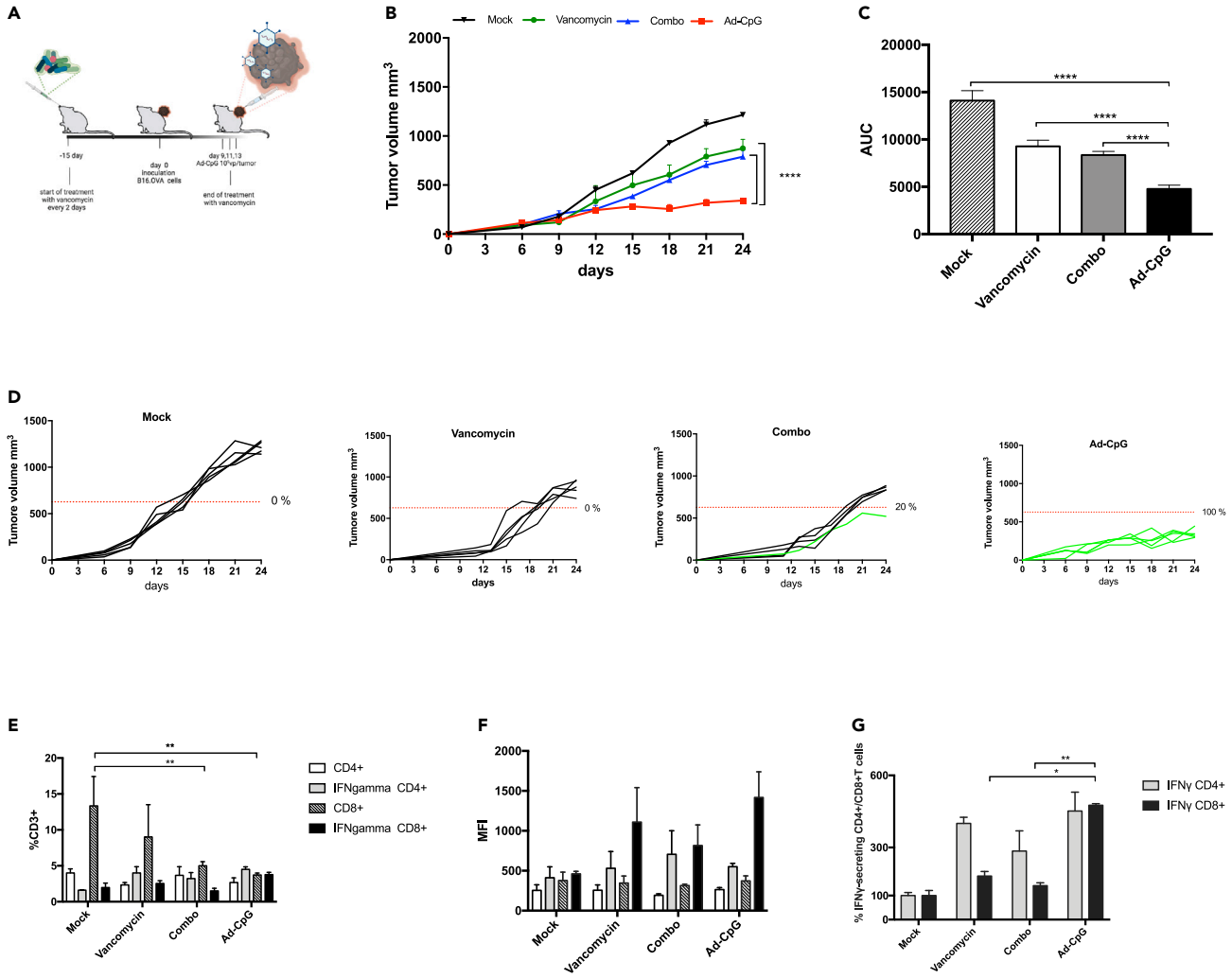

Figure 1. Perturbation of gut microbiome reduces the efficacy of Ad-CpG treatment in a syngeneic mouse model of melanoma

(A) Experimental design: vancomycin was administered by oral gavage every 2 days, starting 15 days before tumor implantation until the first Ad-CpG injection. At day 0, 3.5 × 10^5 B16.OVA cells were injected in the right flank of female C57BL/6J mice (n = 5 per group). Ad-CpG was administered intratumorally on days 9, 11, and 13.

(B) tumor-bearing mice (n = 5 per group) were treated with saline solution (Mock), 100 μL of vancomycin (10 mg/mL) by oral gavage, 1 × 10E9 vp/tumor of Ad-CpG and with a combination of Ad-CpG + vancomycin. Tumor size was determined for each mouse with a digital caliper; results are graphed as mean for each treatment groups +/− standard single error of the mean (SEM); statistical difference has been determined with two-way ANOVA (*p < 0.05; **p < 0.01; ***p < 0.001; p < 0.0001).

(C) Average area under the curves relative to tumor growth in the different experimental groups indicated as mean ± SEM. The statistical significance was evaluated by unpaired t test with Welch's correction and the asterisks indicate statistical significance (****p < 0.0001).

(D) Growth curves for each tumor are reported as a single graph for each group (n = 5 animals per group). The percentage of responders (mice with an absolute tumor volume lower than 627.25 mm^3) for each group is indicated. Volumes of tumors in responders are represented in green, whereas tumors volumes in non-responder are represented by black curves.

(E) Percentages of total $CD3^+$ $CD4^+$ T lymphocytes, IFN-γ $CD4^+$ $CD3^+$, $CD3^+$ $CD8^+$ T lymphocytes and IFN-γ $CD8^+$ $CD3^+$ T cells present in the tumors. The statistical significance was evaluated by two-way ANOVA test using Tukey's multiple comparisons test and the asterisks indicate statistical significance (**p < 0.01) compared to $CD8^+CD3^+$ of tumors in mock-treated mice.

(F) Mean Fluorescent Intensity (MFI) of T cells represented in plot E as average +/− SEM.

(G) Percentages of IFN-γ+ $CD4^+$ $CD3^+$ and IFN-γ+ $CD8^+$ $CD3^+$ T cells calculated as ratio of IFNγ+ $CD4^+$ $CD3^+$/$CD4^+$ $CD3^+$ and ratio IFNγ+ $CD8^+$ CD3+/$CD8^+$ $CD3^+$ and normalized on ratio value of mock group. The statistical significance was evaluated by paired student's t test and the asterisks indicate statistical significance (*p < 0.05; **p < 0.01) compared to the percentage of IFNγ+ $CD8^+$ $CD3^+$ of Ad-CpG-treated tumor. The data are represented as mean ± SEM.

isolated (Figure 2, panel D). Overall survival of mice pre-treated with vancomycin was significantly improved by cohousing (median survival 42.5 days) compared to isolated mice (median survival 23.5 days, p < 0.05, Figure 2, panel E). We then investigated the levels of IFN-γ-producing $CD4^+$ and $CD8^+$ T cells in tumors: interestingly, IFN-γ CD4+/CD4+ T cells ratio in tumors in mice treated with the combined regimen

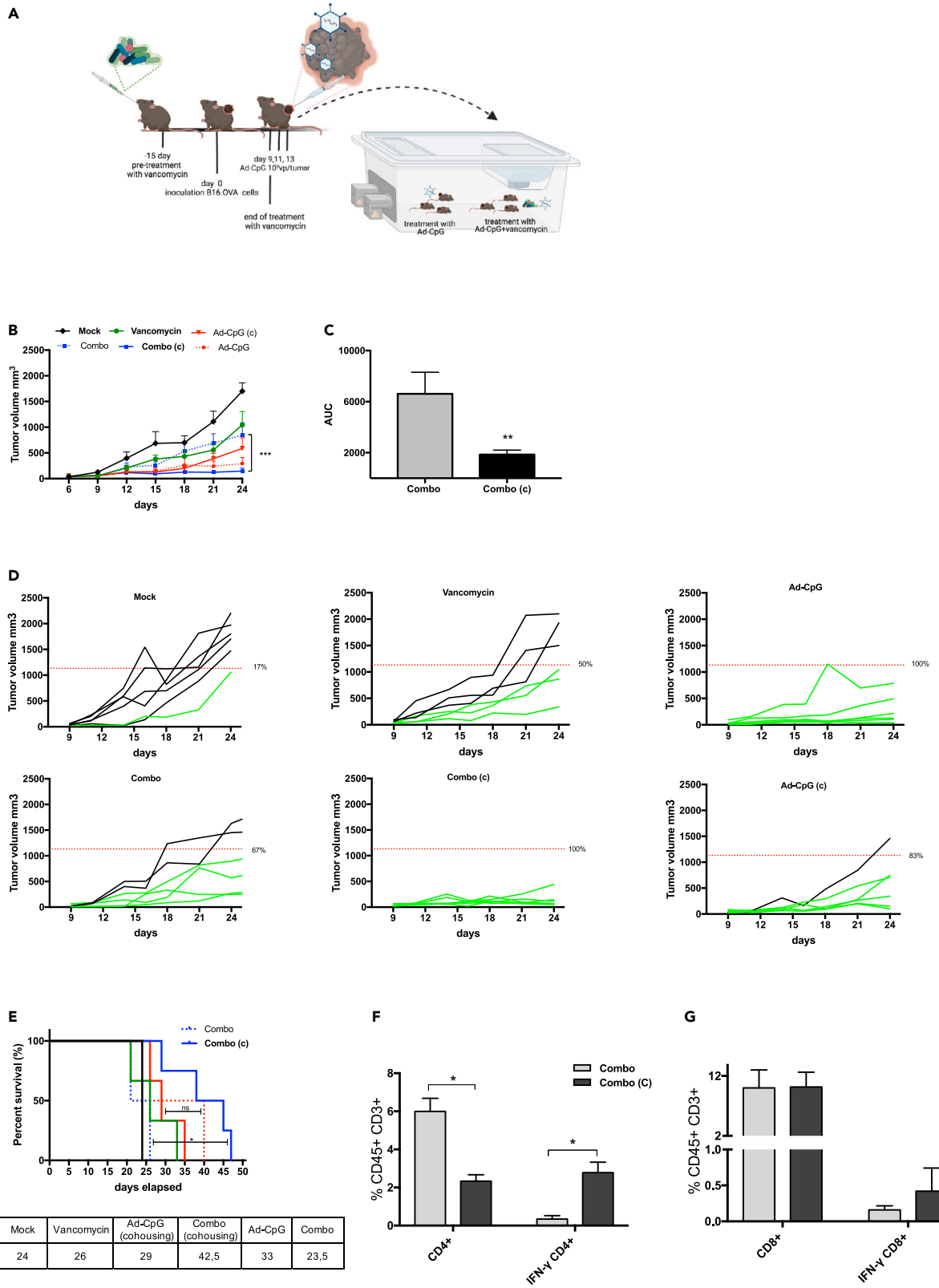

	Mock	Vancomycin	Ad-CpG (cohousing)	Combo (cohousing)	Ad-CpG	Combo
Median survival	24	26	29	42,5	33	23,5

Figure 2. Cohousing with antibiotic-untreated mice can restore Ad-CpG efficacy in vancomycin-treated mice

(A) Experimental design of the cohousing experiment: vancomycin was administered by oral gavage every two days, 15 days before tumor implantation. At day 0, 3.5×10^5 B16.OVA cells were injected in the flank of female C57BL/6J mice (n = 6 per group). Ad-CpG was administered intratumorally on days 9, 11, and 13. After the third injection of the virus, we cohoused the group treated with the combined regimen with mice treated with only Ad-CpG. The groups involved in the cohousing were indicated as (Ad-CpG (c) and (Combo (c). Tumor-bearing mice (n = 6 per group) were treated with saline solution (Mock), 100 μL of 10 mg/mL vancomycin (Vancomycin), 1 × 10E9 vp/tumor of adenovirus (Ad-CpG) and with a combination of Ad-CpG and vancomycin (Combo).

(B) Tumor size was measured with a digital caliper and results are graphed as mean ± SEM; statistical difference has been determined with two-way ANOVA (***$p < 0.001$).

(C) Average area under the curves relative to tumor growth in the different experimental groups is indicated as mean ± SEM; the statistical significance was evaluated by unpaired t test with Welch's correction and the asterisks indicate statistical significance (**$p < 0.01$).

(D) Growth curves for each tumor are reported as a single graph for each group (n = 6 animals per group). Percentage of responders (mice with an absolute tumor volume lower than 1132.22 mm^3) for each group is indicated. The threshold level to evaluate tumor-bearing mice responder to Ad-CpG therapy was defined by the median value of volumes of the saline solution-treated tumors on day 21. Volumes of tumors in responders are represented in green, whereas tumors volumes in non-responders are represented by black curves.

(E) Survival curves relative to the experimental groups represented in panel B. The median survival of each group is reported in the table below the graph. The log rank Mantel-Cox analysis was used to calculate the p value (*$p < 0.05$) of the survival curves.

(F) Percentage of IFN-γ CD4+/CD4+ T cells ratio. The statistical significance was examined by paired student's t test and the asterisks indicate statistical significance (*$p < 0.05$) compared to control group, treated with combined regimen and kept isolated (Combo).

(G) Percentage of IFN-γ CD8+/CD8+ T cells ratio. Results are graphed as mean for each treatment group +/− SEM.

and cohoused was 2.78 compared to a 0.34 ratio observed in tumors from mice treated with the combined regimen and kept isolated (Figure 2, panel F). Similarly, IFN-γ CD8+/CD8+ T cells ratio in tumors from mice treated with a combined regimen and cohoused was significantly higher compared to what was observed in mice treated with a combined regimen and kept isolated (Figure 2, panel G). These data suggest that the perturbation of gut microbiota caused by vancomycin affects levels of IFN-γ-producing $CD8^+$ and $CD4^+$ T cells and that subsequent cohousing with mice that did not receive antibiotic treatment influences microbiota composition, restoring oncolytic virotherapy efficacy.

Bifidobacterium spp. improves Ad-CpG efficacy by reducing tumor-infiltrating T-regs lymphocytes

Recently, investigators have linked abundance of specific bacteria to immunotherapy success.[8–11] In addition, commensal bacteria, such as *Bifidobacterium*, have been shown to modulate dendritic cells (DCs) function resulting in enhanced antitumor T cell activity.[11] We then decided to inoculate syngeneic B16-OVA melanoma cells in female C57BL/6J and treat them with Ad-CpG alone or in combination with a *Bifidobacterium* cocktail (Bifidus) (Figure 3, panel A). We observed an increased response to Ad-CpG therapy in mice that received also Bifidus treatment (Figure 3, panel B) compared to groups treated with Ad-CpG alone and PBS. We observed significantly slower growth kinetics, as represented by the AUC analysis, in mice treated with the combination therapy (Ad-CpG + Bifidus) compared to those treated with Ad-CpG alone (Figure 3, panel C). Interestingly, oral administration of Bifidus by itself resulted in a slightly slower tumor progression compared to mock-treated mice; a different growing trend can be appreciated considering the tumor growth curves for single mouse treated (40% responders, Figure 3, panel D). These surprising results confirmed that Bifidus affects tumor progression and shows a synergistic action with Ad-CpG. Considering the potent immunogenicity of Ad-CpG and the limitation of human serotype 5-based-Ads that do not induce significant oncolysis in murine cells due to species-specific incompatibility, the observed effect most probably relies on the stimulation of the immune system. We analyzed lymphocytes in spleens and tumors collected from all experimental groups. We observed a consistent increase in $CD8^+$ T cells in spleens from mice treated with Bifidus, Ad-CpG, and the combination therapy compared to controls (Figure 3, panel E). No significant differences were appreciated for $CD4^+$ T cells between different treatments; however, a reduced percentage of T-regs lymphocytes was observed in the spleen ($CD4^+$ Foxp3+) and in tumor samples ($CD45^+$CD4+Foxp3+) from mice treated with the combination therapy (Figure 3, panels F–G, respectively) compared to mock group. This reduction is even more significant in mice that received only Bifidus supplementation, suggesting that Bifidus shapes the composition of the gut microbiota and is able to alter the T-regs lymphocytes subset intratumoral infiltration. The quadrant gating strategy that has been used for all samples is reported in supplementary materials (Figures S2–S5). In order to evaluate the presence of immunological memory against the tumor, we collected spleen samples from each group and performed a co-culture assay with B16-OVA cells and preimmunized murine lymphocytes to assess their ability to induce tumor cell death, as previously reported for co-culture-based assays set up to test immunomodulatory agents.[30,31] This experiment is a preliminary assessment of antitumor effect of lymphocytes from mice treated with Ad-CpG, Bifidus, and their combination on cancer cells. The viability of B16-OVA treated with splenocytes derived from mice treated with the combination therapy was significantly lower (56.92% of untreated cells) compared to cells co-cultured with splenocytes collected from mice that received the other treatments (Figure 3, panel H, left plot). This reduced cell survival can be appreciated by images of B16-OVA acquired after splenocytes removal (Figure S6). Cytotoxic effect revealed an increased cell death in cells co-cultured with splenocytes derived from combination therapy-treated mice (Figure 3, panel H, right plot). Despite these preliminary results, we cannot exclude the possibility that the activation of splenocytes collected from Ad-CpG and *Bifidobacterium*-treated mice could be due to a non-specific killing mechanism by T cells activated by the combined regimen.

Treatments with Ad-CpG alone and in combination with Bifidus cause perturbations in mice's fecal microbiome

In order to better characterize the effect of Ad-CpG alone and in combination with Bifidus, we decided to investigate the fecal microbiome profiles of treated mice. We monitored fecal bacterial content over time in treated mice with 16S ribosomal RNAs (rRNAs). Ninety-three fecal

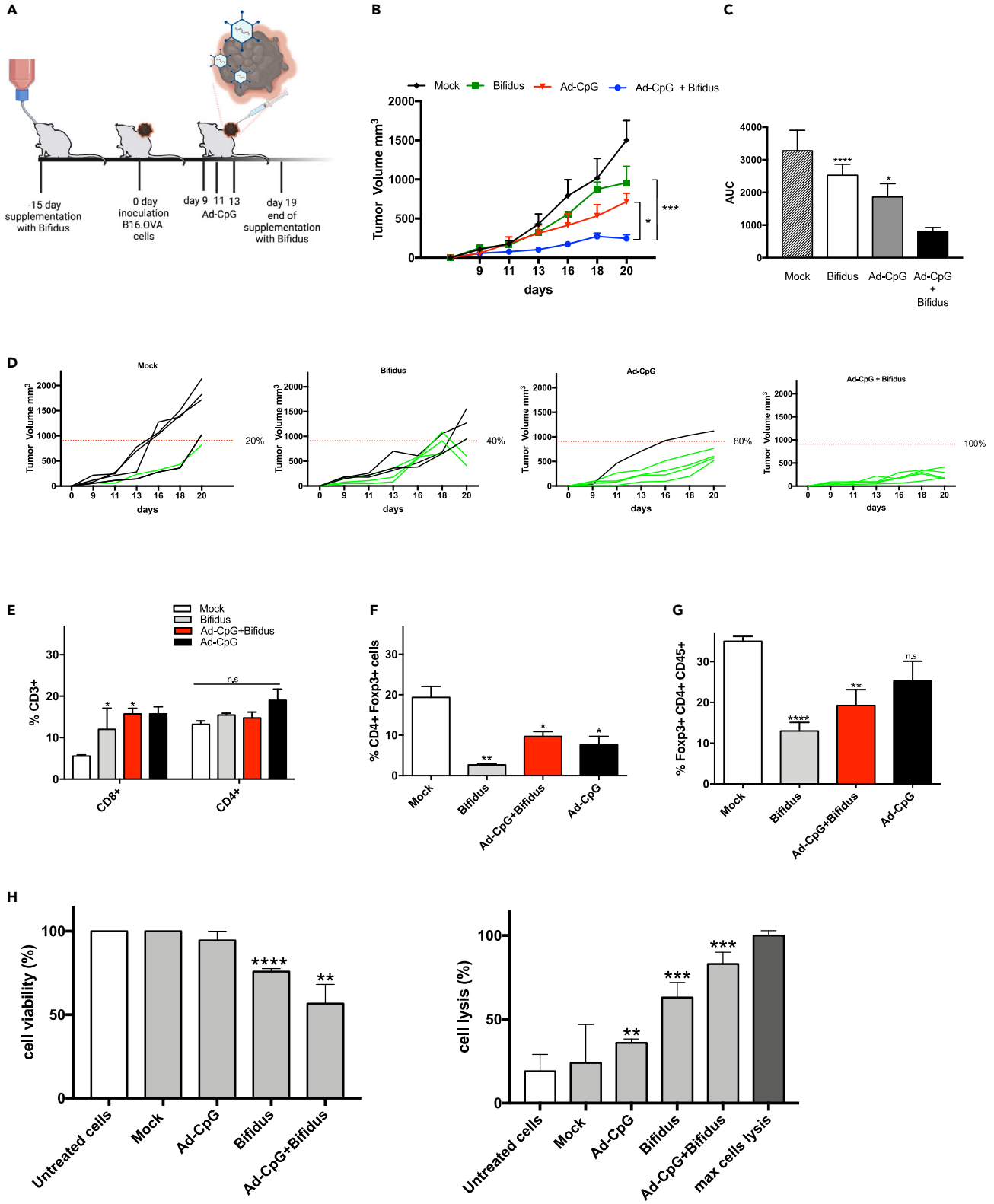
A
-15 day supplementation with Bifidus
0 day inoculation B16.OVA cells
day 9 11 13 Ad-CpG
day 19 end of supplementation with Bifidus
B
Mock
Bifidus
Ad-CpG
Ad-CpG + Bifidus
Tumor Volume mm3
days
C
AUC
Mock
Bifidus
Ad-CpG
Ad-CpG + Bifidus
D
Mock
Bifidus
Ad-CpG
Ad-CpG + Bifidus
20%
40%
80%
100%
E
Mock
Bifidus
Ad-CpG+Bifidus
Ad-CpG
% CD3+
CD8+
CD4+
n,s
F
% CD4+ Foxp3+ cells
G
% Foxp3+ CD4+ CD45+
H
cell viability (%)
Untreated cells
Mock
Ad-CpG
Bifidus
Ad-CpG+Bifidus
cell lysis (%)
max cells lysis

Figure 3. Co-administration of Ad-CpG and *Bifidobacterium* spp. reduces melanoma growth in a syngeneic mouse model by reducing the activity of $CD4^+$ regulatory T cells

(A and B) Experimental design: *Bifidobacterium* spp. cocktail (Bifidus) was added to the drinking water, every 2 days, starting 15 days before the cancer cell inoculation and until day 19. At day 0, 3.5×10^5 B16.OVA cells were injected in the right flank of female C57BL/6J mice (n = 5 per group). Ad-CpG was administered intratumorally on days 9, 11 and 13; B) tumor-bearing mice (n = 5 per group) were treated with saline solution (Mock), 10E9 CFU/mL of Bifidus (Bifidus), 1 × 10E9 vp/tumor of adenoviral therapy (Ad-CpG) and with a combination of the two monotherapies (Ad-CpG + Bifidus). Tumor size was determined for each mouse; results are graphed as mean for each treatment group +/− SEM; the statistical difference has been determined with two-way ANOVA (*p < 0.05; ***p < 0.001).

(C) Average area under the curves relative to the tumor growth in the different experimental groups is indicated as mean ± SEM. The statistical significance was evaluated by unpaired t test with Welch's correction and the asterisks indicate statistical significance (*p < 0.05; ***p < 0.001).

(D) Growth curves for each tumor reported as a single graph for each group (n = 5 animals per group). The percentage of responders (mice with an absolute tumor volume lower than 907.91 mm^3) for each group is indicated. Volumes of tumors in responders are represented in green, whereas tumors volume in non-responders are represented by black curves.

(E) Percentage of total $CD3^+$ $CD4^+$ T-lymphocytes present in the spleen of treated mice.

(F) Percentage of total $CD3^+$ $CD4^+$ Foxp3+ T-lymphocytes present in the spleens.

(G) Percentage of total $CD45^+$ $CD4^+$ Foxp3+ T lymphocytes present in the tumors. The statistical significance was evaluated by Student's *t* test and the asterisks indicate statistical significance (*p < 0.05; **p < 0.01; ***p < 0.001; ****p < 0.0001) compared to the relative lymphocytes' population of spleens or tumors in mock-treated mice.

(H) B16-OVA cells were incubated with or without murine splenocytes isolated from spleens of mice, previously treated with PBS (mock), Ad-CpG, Bifidus or a combination of virus and *Bifidobacterium* for 48 h. Left plot: cell viability is reported as a percentage of viable cells compared to untreated B16-OVA cancer cells (white bar). Right plot: tumor cell lysis was determined by measurement of the LDH levels released in the culture medium and expressed as a percentage with respect to max lysis control represented by cells treated with 10% Triton X-100. The experiments were performed in triplicate and statistical significance (*p < 0.05; **p < 0.01; ***p < 0.001; ****p < 0.0001) was assessed by the Student's t test by comparing the cells, treated as indicated, to untreated cells. The data are represented as mean +/− standard deviation (SD).

samples were collected and processed for microbiome evaluation in a single next-generation sequencing (NGS) run. In order to investigate a possible link between gut microbiome composition and the different therapeutic regimens, we sought to investigate differences between the microbial profiles of groups. Alpha diversity plots showed that the microbial richness, measured by observed operational taxonomic unit (OTU), Chao1, and Shannon indices, does not differ between treatments or time points (Figure S7). Beta diversity analysis performed to test the inter-group variability showed that the combination of time and treatment explained a significant proportion of the variation in the microbial community. The statistical difference was evaluated by PERMANOVA (Adonis) statistical test using both weighted (p = 0.001, R2 = 0.449) and unweighted (p = 0.001, R2 = 0.31) UniFrac distance. (Figure S8, panels A–B). According to the Kruskal-Wallis test among the four times points for each treatment, distinct phyla were identified such as Verrucomicrobia, Tenericutes, Proteobacteria, Fusobacteria, Firmicutes, Deferribacteres, Cyanobacteria, Bacteroidetes, and Actinobacteria (Figure 4, panel A). In the untreated group (Mock), Tenericutes (p < 0.001) and Actinobacteria (p < 0.001) were significantly different between the four time points whereas, in the Bifidus-treated group, significant differences were observed in Proteobacteria, Cyanobacteria, and Actinobacteria. On the other hand, in the group treated with Ad-CpG, Firmicutes and Actinobacteria were significantly different between the four time points; in the group treated with Ad-CpG and Bifidus, additional phyla Tenericutes, Deferribacteres, and Cyanobacteria were identified (Figure 4, panel A). Interestingly, the fecal microbiota of both groups (Ad-CpG and Ad-CpG and Bifidus) treated with Ad-CpG was characterized by a significant abundance of phyla Firmicutes and Actinobacteria; specifically considering the time point Day 18, the relative abundance of Firmicutes phylum was about 63% in both groups treated with adenoviral therapy (Figure 4, panel A).

By using Dunn's test, a post hoc non-parametric test applied to the Kruskal-Wallis significant amplicon sequence variants (ASVs), we performed multiple pairwise tests in order to identify between which time pairs the phyla differentially abundant were significant. As reported in Table S1, Tenericutes and Actinobacteria phyla abundances resulted significantly different between the earlier (Day −10) and later (Day 18 and Day 20) time points suggesting that their relative abundance was independent of tumor growth both in mock and Bifidus-treated groups. In both groups treated with Ad-CpG, the abundance of Actinobacteria was significantly different between Day −10 to Day 18, indicating that the pre-treatment with Bifidus did not affect its richness. In the Ad-CpG-treated group, Firmicutes phylum was differentially abundant between Day 0 and Day 18, when differences between tumor growth curves were well appreciated, as shown in Figure 3, panel B. A similar result was confirmed in the group treated with Ad-CpG and Bifidus, in which the relative abundance of the Firmicutes was different also between Day −10 and the endpoint (Day 20) (Table S1). These data confirmed that melanoma-bearing mice treated with Ad-CpG were characterized by an enrichment of Firmicutes in their fecal microbiota. The relative abundance of differentially abundant genera (p < 0.05) for each study group, according to the Kruskal-Wallis test among the four time points, was shown in Figure 4, panel B.

In fecal bacterial content of mice treated with Ad-CpG, the genera identified were *Ruminiclostridium_9, Ruminiclostridium, Roseburia, Lachnospiraceae_UCG-001*, *Lachnospiraceae_NK4A136*, and *Faecalibaculum*. All these bacterial genera belong to the *Firmicutes* phylum. In addition to these genera, *Turicibacter*, *Oscillibacter*, and *Lachnoclostridium* were identified in the group treated with Ad-CpG plus Bifidus. *Bifidobacterium*, belonging to the Actinobacteria phylum, was identified in all groups, but with a relative abundance of about 10% in the group treated with Bifidus (Day 20), compared to a relative abundance of 4.9% observed in the group treated with Ad-CpG and Bifidus (Day 20) (Figure 4, panel B).

At genus level, we have identified a specific fecal microbiota profile in both groups treated with Ad-CpG and with Ad-CpG and Bifidus (Figure 5, panels A and B). Specifically, *Bifidobacterium, Faecalibaculum*, and *Lachnospiraceae_NK4A136* genera showed a relative

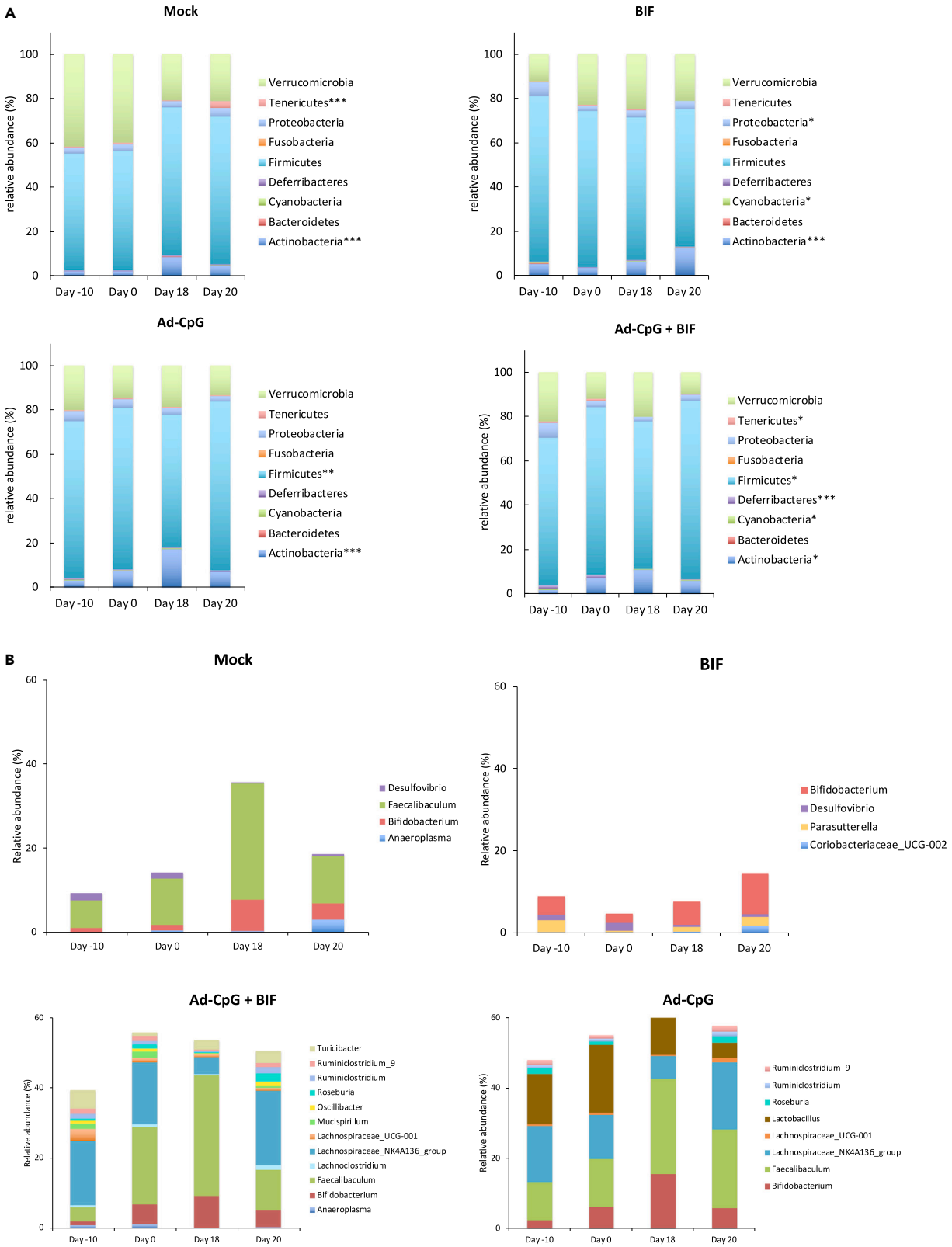
A
Mock
relative abundance (%)
100
80
60
40
20
0
Day -10
Day 0
Day 18
Day 20
Verrucomicrobia
Tenericutes***
Proteobacteria
Fusobacteria
Firmicutes
Deferribacteres
Cyanobacteria
Bacteroidetes
Actinobacteria***
BIF
relative abundance (%)
Verrucomicrobia
Tenericutes
Proteobacteria*
Fusobacteria
Firmicutes
Deferribacteres
Cyanobacteria*
Bacteroidetes
Actinobacteria***
Ad-CpG
relative abundance (%)
Verrucomicrobia
Tenericutes
Proteobacteria
Fusobacteria
Firmicutes**
Deferribacteres
Cyanobacteria
Bacteroidetes
Actinobacteria***
Ad-CpG + BIF
relative abundance (%)
Verrucomicrobia
Tenericutes*
Proteobacteria
Fusobacteria
Firmicutes*
Deferribacteres***
Cyanobacteria*
Bacteroidetes
Actinobacteria*
B
Mock
Relative abundance (%)
60
40
20
0
Day -10
Day 0
Day 18
Day 20
Desulfovibrio
Faecalibaculum
Bifidobacterium
Anaeroplasma
BIF
Relative abundance (%)
Bifidobacterium
Desulfovibrio
Parasutterella
Coriobacteriaceae_UCG-002
Ad-CpG + BIF
Relative abundance (%)
Turicibacter
Ruminiclostridium_9
Ruminiclostridium
Roseburia
Oscillibacter
Mucispirillum
Lachnospiraceae_UCG-001
Lachnospiraceae_NK4A136_group
Lachnoclostridium
Faecalibaculum
Bifidobacterium
Anaeroplasma
Ad-CpG
Relative abundance (%)
Ruminiclostridium_9
Ruminiclostridium
Roseburia
Lactobacillus
Lachnospiraceae_UCG-001
Lachnospiraceae_NK4A136_group
Faecalibaculum
Bifidobacterium

Figure 4. Treatment of tumor with Ad-CpG increases Firmicutes in murine fecal microbiome

(A) The bar plots show Kruskal-Wallis test results on amplicon sequence variants (ASVs) grouped in phyla for each study group over the time points (Day-10, Day 0, Day 18, and Day 20). The treatments were indicated as Mock: untreated tumor-bearing-mice; BIF: *Bifidobacterium* oral supplementation-receiving mice; Ad-CpG: Ad5-CpG-treated mice; Ad-CpG + BIF: combined regimen-treated mice. Each column in the plot represents a time point and each color in the column represents the percentage of relative abundance. The phyla significantly (*$p < 0.05$; **$p < 0.01$; ***$p < 0.001$) different between the four time points and for each treatment, were shown in each panel alongside each bar plot graph.

(B) The bar plots show the relative abundances of differentially abundant genera ($p < 0.05$) according to the Kruskal-Wallis test among the four time points for each treatment. The color legends show the identified genera.

abundance greater than 2% in fecal bacterial composition in groups treated with Ad-CpG. These data support the hypothesis that groups treated with Ad-CpG alone and in combination with Bifidus, for which we obtained higher antitumoral efficacy, were characterized by a specific fecal microbiota composition.

Bifidobacterium-derived peptides stimulate antitumor responses via T cell cross-reactivity with melanoma-derived antigens

Considering that the supplementation with Bifidus in melanoma-bearing mice resulted in a slightly slower tumor progression compared to the control group, and in an increased response to Ad-CpG treatment, we decided to investigate a possible underlying mechanism that could explain the immunomodulatory activity of Bifidus linked to tumor regression. We hypothesized that several *Bifidobacterium*-derived peptides highly similar to melanoma epitopes could trigger a more effective antitumoral CTL response.

To this end, we compared the peptidome of the B16.F10 melanoma cell line with that of all *Bifidobacterium* species, including those present in the commercial cocktail used for *in vivo* supplementation, using Hamming similarity measure and Homology Evaluation Xenopeptides (HEX) platform, as represented by Figure 6, panel A. We selected *Bifidobacterium* peptides differing by up to three amino acid residues from the melanoma peptides, and after refinement, using the alignment and affinity binding scores by HEX, we obtained a list of ten *Bifidobacterium* peptides and fourteen melanoma peptides (Table 1). First, all *Bifidobacterium* peptides were tested *in vivo,* and in particular, each group of mice received a primary and a boosting dose of two *Bifidobacterium* peptides (B) complexed with the poly (I:C) adjuvant. Secondly, the corresponding highly similar melanoma peptides (T) to peptides B were tested *in vitro* by the IFN-γ ELISpot assay, as shown in the schematic representation of the immunization regimen (Figure 6, panel B). Splenocytes collected from mice preimmunized with peptides RQYGFIVL (B1) and RILKFLFL (B2) (indicated as B1+B2 group in the plot) showed a significant increase of IFN-γ CD8 T cells when re-stimulated singularly with peptide B1 ($p < 0.01$) and B2 ($p < 0.05$), compared to control groups treated with PBS or poly (I:C) adjuvant (Figure 7, panel A), confirming their stimulatory activity (legend of peptides indicated in Table 1).To assess the levels of immunogenicity of tumor peptides, we pulsed the preimmunized splenocytes of the B1+B2 group, with corresponding similar tumor peptides: T1, T5, T2, and T6. The first induced an IFN-γ production similar to that observed in the poly (I:C) control group; instead, stimulation with tumor peptides T5 and T6 increased the IFN-γ production more than that in control groups and for T2 no response was detected (Figure 7, panels B–C).Then, splenocytes harvested from preimmunized mice pulsed with B2 and T5 (bars in the magenta box) (Figure 7, panel D) exerted similar immunological activity *in vitro* and *in vivo*, confirming that the molecular mimicry between the bacterial peptides and tumor antigens can increase antitumor immunity. Additionally, a significantly increased immune activation was observed in pulsing splenocytes with tumor peptide T6 ($p < 0.0001$) (bar in the green box) than peptides investigated and control group preimmunized with PBS (Figure 7, panels D–E). To confirm the level immunogenicity of described peptide B2 and evaluate whether tumor peptides T5 and T6 were indeed immunogenic as B2, we harvested splenocytes from groups treated with vancomycin and with oral supplementation of Bifidobacterium spp. (Bifidus) and pulsed with peptides B2, T5, and T6. An additional group treated with PBS was used as a control group. Vancomycin-mediated microbiota perturbation significantly affected the response to peptides B2 compared to the Bifidus-treated group ($p < 0.01$), as shown by reduced immune activation (Figure 7, panel F). Therefore, we confirmed that gut microbiota perturbation negatively affects response to Ad-CpG therapy, as described in Figure 3, but also to B2 peptide. Splenocytes from mice pre-treated with Bifidus and stimulated with tumor peptides T5 and T6 showed a slightly increased trend of activation, although not achieving full statistical significance, compared to the group treated with vancomycin (Figure 7, panel F). Finally, we preimmunized mice only with peptide B1 and pulsed the splenocytes *in vitro* with the last two peptides, SQYRFIVF (T3) and RGYEFIVR (T4). Peptide T3 was able to elicit a significantly major immune response than other peptides (Figure S9, panels A and B).

All these results strongly confirmed our initial hypothesis, according to which a T cell cross-reactivity occurs between highly immunogenic *Bifidobacterium*-derived epitope and melanoma antigens restricted to major histocompatibility complex (MHC)-I. These shared peptides could be deeply exploited to design powerful and cancer-specific OVs-based therapeutic vaccines, increasing their antitumoral effect.

DISCUSSION

Despite the clinical impact of ICIs in cancer therapy, accumulating evidence suggests that these therapeutic agents show some limitations: only a fraction of patients benefit from ICIs treatment that is ineffective against immunologically "cold" tumors characterized by low TILs count.[21] To this end, OVs represent attractive therapeutic agents that can be combined with ICIs, increasing their response blockade in poorly immunogenic tumors.[21,23,25] Variability in the observed response rate is also due to environmental and genetic factors: intestinal microbiota has been indicated as a cause of variability in response to ICIs because of its general immunomodulatory action. Considering OVs therapy as a possible complement to increase the success of ICIs immunotherapy, we decided to investigate whether intestinal microbiota could affect OVs therapy efficacy.

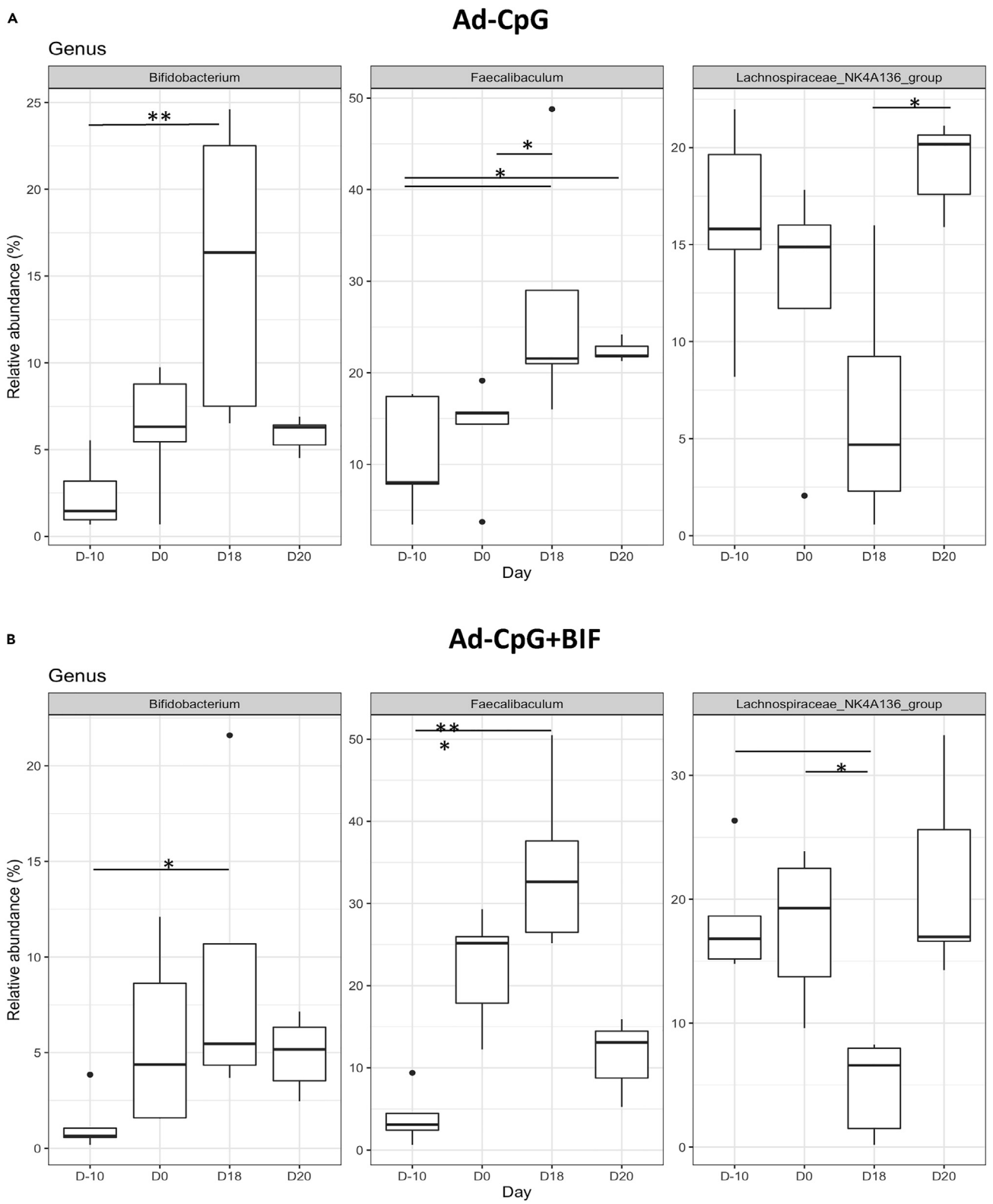

Figure 5. Treatment of tumor with Ad-CpG increases the abundance of three specific genera in murine fecal microbiome

(A and B) Over the time points (Day-10, Day 0, Day 18, and Day 20), the three genera with a relative abundance >2% shown in the boxplots were in common between Ad-CpG and Ad-CpG + BIF group and belong to phyla Actinobacteria (*Bifidobacterium*) and Firmicutes (*Faecalibaculum and Lacknospiraceae*

Figure 5. *Continued*

NK4A136). The treatments were indicated as Ad-CpG: Ad5-CpG-treated mice; Ad-CpG + BIF: combined regimen-treated mice. Middle line in boxes represents the median; lower box bounds the first quartile; upper box bounds the 3rd quartile. Whiskers represent the 95% confidence interval of the mean. The significance of distribution differences has been calculated by applying the Kruskal-Wallis test, Dunn's post-hoc test and Benjamini-Hochberg p value adjustment (*$p < 0.05$; **$p < 0.01$; ***$p < 0.005$).

We used an oncolytic adenovirus enriched with CpG island as OV for this study.[24] Ad-CpG has been successfully evaluated in the past using a syngeneic melanoma model based on the inoculation of B16-OVA cells in C57BL/6J mice; this melanoma model responds to ICIs therapy and is sensitive to microbiota perturbation.[32,33] In order to evaluate whether gut microbiota was necessary to the antitumoral activity of the Ad-CpG, we reduced intestinal bacterial diversity, pre-treating mice with the antibiotic vancomycin, which has been previously used for the same purpose by Vetizou et al.[10,34]

We found that pre-treatment with vancomycin reduced the efficacy of Ad-CpG therapy: mice had a faster tumor progression compared to mice treated only with Ad-CpG (Figure 1, panel B). We can therefore conclude that bacterial diversity in general is necessary for the efficacy of Ad-CpG therapy. In fact, vancomycin-based bacterial depletion induced an alteration of antitumoral immune response leading to a reduced count of IFN-γ+CD8$^+$ TILs. In order to further confirm that bacterial depletion was the cause of the poor efficacy of Ad-CpG in vancomycin-treated mice, we cohoused a group of mice pre-treated with vancomycin and then treated with Ad-CpG (combined regimen) with a group of mice that did not receive any antibiotics. Cohousing is supposed to reduce or abrogate microbiota differences in the two groups because of mice coprophagy and grooming behavior[35]; transmission of the gut microbiota, by cohousing, significantly reduced differences efficacy of Ad-CpG therapy in mice pre-treated with vancomycin and mice that did not receive any antibiotics (Figure 2, panels B–C). These results confirmed that microbial diversity is relevant for the efficacy of Ad-CpG treatment in this melanoma model; in fact, mice pre-treated with vancomycin and kept isolated showed reduced survival (Figure 2). Cohousing-mediated improvement of Ad-CpG efficacy was also accompanied by an increase of tumor-infiltrating IFN-γ CD4$^+$ and IFN-γ CD8$^+$ T cells, underlining the effect of intestinal microbiota on the immune response against melanoma in this model.

Mounting evidence has demonstrated the effects of the gut microbiota on the efficacy of ICIs in humans and mice;[4,8,36] specifically favorable gut bacteria increase the population of CD8$^+$ T cells and decrease T-regs within the tumor bed.[36] As reported, beneficial commensal *Bifidobacterium* boosts the efficacy of the PD-1/PD-L1 blockade by activating DCs and tumor-specific CD8$^+$ T cells.[11] Therefore, we evaluated a possible immunomodulatory activity of Bifidus supplementation, combined with Ad-CpG therapy, in our melanoma mouse model. Our data strongly indicate that Bifidus supplementation increased the response to Ad-CpG compared to mice that did not receive this probiotic. We observed fewer tumor-infiltrating T-regs in mice that received Bifidus supplementation; these lymphocytes are well known to exert an immunosuppressive action. Thus, Bifidus supplementation increases the efficacy of Ad-CpG treatment by modulating antitumoral immune response and, more specifically, by reducing the presence of immune suppressive lymphocytes and increasing intratumoral CTLs compared to the control group treated with virus alone. Therefore, Bifidus supplementation was able to boost the immunovirotherapy efficacy (Figure 3). As proof of this, splenocytes harvested from vaccinated mice with Ad-CpG and Bifidus cause extensive T cell-mediated killing of melanoma cells. We believe that this preliminary assessment of T cell-mediated tumor killing and then of immunological memory could not be directly connected to the presence of viral therapy combined with Bifidus supplementation.

Based on these observations, our data indicate that the immune-mediated eradication of melanoma, exerted by Ad-CpG, was affected by intestinal microbiota composition. As previously shown, antibiotic-mediated gut microbiota alteration reduces some beneficial bacteria taxa altering intestinal anti-inflammatory and immunomodulatory properties.[10] These bacterial communities contribute to a healthy host-microorganism balance useful to optimally perform metabolic and immune functions and reduce disease development. The phylogenetic composition of the bacterial communities in both humans and mice seems to be similar at the phylum level, where the two main bacterial phyla of the murine intestinal tract are the Bacteroidetes and the Firmicutes,[37,38] the most predominant phyla in a human healthy gut.[39] For this reason, we compared fecal microbiome of mice treated with a combined regimen (Ad-CpG + Bifidus) to that of mice that received a single treatment and a control group, by DNA sequencing of the 16S rRNA gene in bacteria. Ad-CpG and combined regimen-recipient mice showed a predominance of the Firmicutes and Actinobacteria phyla in their fecal bacterial content showing, respectively, seven and nine genera belonging to the Firmicutes phylum (Figure 4). Specifically, groups treated with Ad-CpG showed, in their fecal bacterial content, three genera *Lachnospiraceae_NK4A136* (14,5%), *Faecalibaculum* (18%), and *Bifidobacterium* (13%) with a relative abundance >2% belonging to phyla Actinobacteria and Firmicutes, respectively (Figure 5).

Therefore, we had evidence that Ad-CpG treatment, as a stand-alone and in combination with Bifidus, affects fecal microbiota composition. The enrichment of the phylum Firmicutes in the gut microbiota of Ad-CpG-treated groups is likely to create a favorable and immunologically permissive gut microbiota that contributes to the antitumoral immune responses.

In order to understand how gut microbiota exerts antitumor effects, we hypothesized that the molecular mimicry between antigens expressed by melanoma cells and antigens derived from peptides of *Bifidobacterium* could be responsible for the synergistic effect observed in groups treated with a combined regimen. To this end, we compared the peptidome of melanoma cell line B16.F10 with that of all *Bifidobacterium* species, as described in the schematic representation of the immunization regimen (Figure 6). Fourteen MHC I-restricted melanoma murine peptides extremely similar to peptides expressed in proteins from *Bifidobacterium* species were identified and then tested *in vivo* and *in vitro*. As reported by IFN-γ ELISpot assay, re-stimulation of *Bifidobacterium* (B1+B2) preimmunized splenocytes with peptides B1 and B2 induced an increased IFN-γ CD8 T cells, confirming the immunomodulatory potential of both peptides (Figure 7, panel A). Despite the high similarity between *Bifidobacterium* B1 and melanoma peptides T1 and T2, no significant differences were appreciated in the number

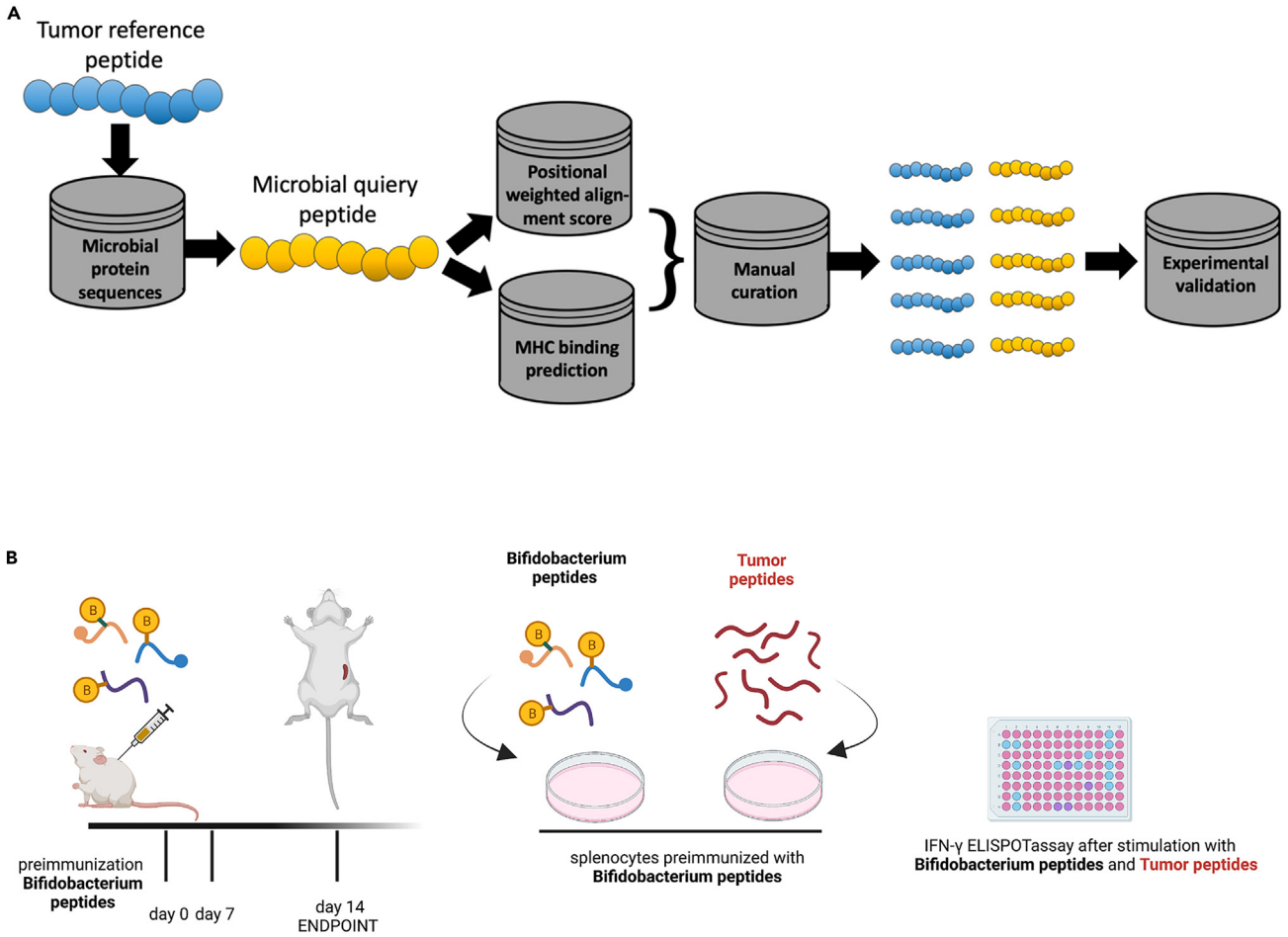

Figure 6. Experimental characterization of peptides

(A) Flowchart of the bioinformatics workflow for peptides discovery.

(B) Schematic representation of the schedule followed during the preimmunization procedure. The mice have been subcutaneously injected with two *Bifidobacterium* peptides (such as B1+B2) at days 0 and 7. PBS or poly (I:C) were used as controls as well. The spleens were harvested at day 14 and IFN-γ ELISpot was performed on harvested splenocytes and individual response to *Bifidobacterium* peptides and the corresponding similar tumor peptides were evaluated for each mouse.

of spots IFN-γ. Surprisingly, stimulation of B1+B2 preimmunized splenocytes, with specific melanoma epitopes T5 and T6, induced an increased IFN-γ CD8 T cells, indicating a mechanism of T cells cross-reactivity, based on possible molecular mimicry mechanism (Figure 7, panels D magenta and green boxes). One of the most interesting findings is that the specific epitope B2 (RILKFLFL) derived from peptides of *B.breve* and *B.longum* is efficiently presented on cell surface and triggers specific T cell responses; in addition, melanoma epitope T6 (RILKFLQL) is highly immunogenic and induces *in vitro* a greater amount of effector T cells that are cross-reactive with the B2 antigen. In the present study, for the first time to our knowledge, a possible association between the gut microbiota and the OVs therapy has been explored. The identification and use of specific antigens of *Bifidobacterium*, similar to melanoma antigens, for immunovirotherapy, has to be carefully considered. Antigens selection could be useful to optimize the manipulation of OVs, expanding OVs potency and reducing the variability of clinical outcomes. The effect of these modifications could be further enhanced by supplementation with *Bifidobacterium* species related to antigens selected, favoring a targeted bacterial colonization that positively affects the response to cancer immunotherapy. Then, results obtained could open up new perspective to design powerful anticancer OVs-based vaccines obtaining even more durable clinical benefits.

Limitations of the study

The present study is limited to an oncolytic adenovirus in a specific syngeneic mouse model of melanoma; therefore, further studies will be necessary to evaluate the role of intestinal microbiota and its possible perturbations in other tumor models and with additional OVs and, finally, in clinical settings. In addition, role of metabolites and other bacterial components has to be taken into account and will be part of

Table 1. *Bifidobacterium* and melanoma peptides

B16.F10 peptides (Reference)	Microbial peptides (Query)	*Bifidobacterium* species	Hamming distance	weighted alignment score	H-2Kb binding affinity (nM)
AVLKYYKV	ASLKYYKV	bifidum	1	269	40.4
TAYEFAKL	TMYEFAKL	longum	1	259	2.5
SGYIPARL	SKYIPARL	breve, longum, bifidum	1	256	181.9
SNYERLESL	SNYERLEFL	breve, bifidum	1	254	54.4
ISLEFRNL	IALEFRNL	longum	1	246	3
KILTFDQL	KGLTFDQL	longum	1	244	136.7
SGYKFGVL	SGYKFDVL	lactis	1	225	12.4
VSTKFEHL	VSTKFSHL	longum	1	220	4.8
RQYIFSKL T1	RQYGFIVL B1	breve	3	86	156.65
RQYMFSSL T2	RQYGFIVL B1	breve	3	99	156.65
SQYRFIVF T3	RQYGFIVL B1	breve	3	168	156.65
RGYEFIVR T4	RQYGFIVL B1	breve	3	158	156.65
RILKFLKL T5	RILKFLFL B2	breve, longum	1	226	67.2
RILKFLQL T6	RILKFLFL B2	breve, longum	1	226	67.2

Tables 1.List of ten Microbial peptides (query) differing by up to three amino acid residues from the fourteen B16.F10 peptides (reference). The different residue between reference sequence and query sequence is indicated in bold font. The legend of peptides is indicated below the reference and query sequences. The query peptide B1 is similar to four reference peptides: T1, T2, T3, and T4 (Hamming distance = 3). The query peptide B2 is similar to two reference peptides: T5 and T6 (Hamming distance = 1). The microbial peptides belong to different *Bifidobacterium* species, indicated in the third column. The distance of amino acid residues between query and reference are indicated by the hamming distance value; the weighted alignment score and the H-2Kb affinity binding scores were refined by software HEX.

a further investigation. Therefore, exploitation of the potential of the OV immunotherapy-gut microbiome axis has to be further examined to further improve the efficiency of this therapeutic strategy.

STAR★METHODS

Detailed methods are provided in the online version of this paper and include the following:

- KEY RESOURCES TABLE
- RESOURCE AVAILABILITY
  - Lead contact
  - Materials availability
  - Data and code availability
- EXPERIMENTAL MODEL AND STUDY PARTECIPANT DETAILS
  - Animal experiments
  - Tumor implantation and tumor growth measurement
  - Virus administration
  - Antibiotic and *bifidobacterium* treatment
- METHOD DETAILS
  - Cell lines and reagents
  - Virus production
  - Tumor cell lysis assays
  - Isolation of immune cells from mice spleen and tumor
  - Flow cytometry analysis
  - IFN-γ ELISpot

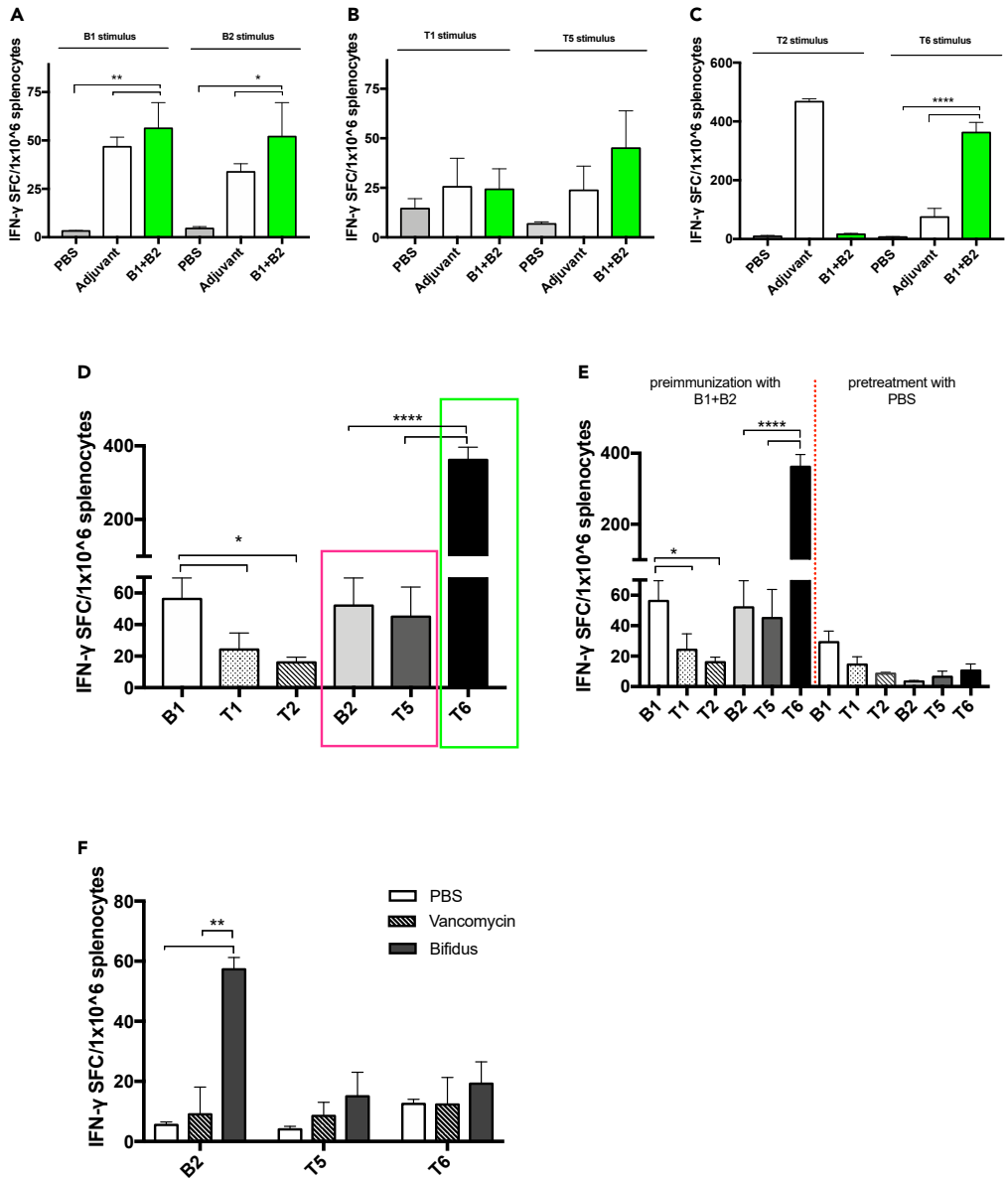

Figure 7. *Bifidobacterium*-derived peptides can resemble murine melanoma epitopes and mediate strong CTL response

(A–E) IFN-γ ELISpot was performed on harvested splenocytes from mice preimmunized with PBS, adjuvant poly (I:C) or with two *Bifidobacterium* peptides (B1+B2) and individual response to B1 stimulus and B2 (B) to T1 and T5 stimulus (C) to T2 and T6 stimulus (D) to stimulus B1, T1, T2, B2, T5, and T6 for each group of mice (n = 3) is reported as the value of IFN-γ spot-forming cells (SFC) on 1 × 10^6 splenocytes. Comparison of number of spots IFN-γ detected between B2 and T5, in magenta box, and comparison between B2 and T6 in the green box (E) IFN-γ ELISpot was performed on harvested splenocytes from mice preimmunized with two *Bifidobacterium* peptides (B1+B2) and with PBS and stimulated with peptides B1, T1, T2, B2, T5, and T6.

(F) IFN-γ ELISpot was performed on harvested splenocytes from mice treated with PBS, with vancomycin and from mice received oral supplementation with *Bifidobacterium* spp. (Bifidus) and stimulated with peptides B2, T5, and T6. For each group of mice (n = 3) number of spots (IFN-γ) is reported. All data are depicted as bar plots and represented as mean ± SEM. The statistical analysis was performed with ordinary one-way ANOVA test (*p < 0.05; **p < 0.01; ***p < 0.001; ****p < 0.0001).

SUPPLEMENTAL INFORMATION

Supplemental information can be found online at https://doi.org/10.1016/j.isci.2023.107668.

ACKNOWLEDGMENTS

The authors thank Dr. Silvia Esposito, veterinary doctor responsible for the welfare of animals of animal facility of CEINGE Biotecnologie Avanzate Franco Salvatore, and Dr. Flavio Starnone for their valuable help and for sharing their extensive professional expertise. Professor Lucio Pastore is supported by funding of Italian Natural Recovery and Resilience Plan (PNRR) and POR Campania FESR 2014/2020: Sviluppo di Approcci Terapeutici INnovativi per patologie neoplastiche resistenti ai trattamenti (SATIN). Professor Vincenzo Cerullo is supported by funding of Italian Natural Recovery and Resilience Plan (PNRR), the European Research Council under the European Union's Horizon 2020 Framework program (H2020)/ERC-CoG-2015 Grant Agreement No. 681219, the Helsinki Institute of Life Science (HiLIFE), the Jane and Aatos Erkko Foundation (decision 19072019), the Cancer Society of Finland (Syöpäjärjestöt).

AUTHORS' CONTRIBUTIONS

LT, SF, MP, CC, LC, and MV performed *in vitro* and *in vivo* experiments; GS and LG contributed to flow cytometry analyses; IG, MRG, and VDA contributed to 16S rRNA microbiome sequencing and data processing and interpreted the results; CDL, GC, and VDA contributed to experiment design; TW and BS contributed to discovery peptide analyses; LT, SF, VC, and LP designed the study, interpreted the results, and contributed to manuscript writing. All authors read, corrected, and approved the final manuscript.

DECLARATION OF INTERESTS

Vincenzo Cerullo is founder and shareholder at VALO therapeutics.

Received: May 12, 2023
Revised: July 13, 2023
Accepted: August 16, 2023
Published: August 19, 2023

REFERENCES

1. Kim, K., Kim, H.S., Kim, J.Y., Jung, H., Sun, J.-M., Ahn, J.S., Ahn, M.-J., Park, K., Lee, S.-H., and Choi, J.K. (2020). Predicting clinical benefit of immunotherapy by antigenic or functional mutations affecting tumour immunogenicity. Nat. Commun. *11*, 951. https://doi.org/10.1038/s41467-020-14562-z.
2. Sambi, M., Bagheri, L., and Szewczuk, M.R. (2019). Current Challenges in Cancer Immunotherapy: Multimodal Approaches to Improve Efficacy and Patient Response Rates. J. Oncol. *2019*, 4508794. https://doi.org/10.1155/2019/4508794.
3. Alexander, J.L., Wilson, I.D., Teare, J., Marchesi, J.R., Nicholson, J.K., and Kinross, J.M. (2017). Gut microbiota modulation of chemotherapy efficacy and toxicity. Nat. Rev. Gastroentero. *14*, 356–365. https://doi.org/10.1038/nrgastro.2017.20.
4. Gopalakrishnan, V., Spencer, C.N., Nezi, L., Reuben, A., Andrews, M.C., Karpinets, T.V., Prieto, P.A., Vicente, D., Hoffman, K., Wei, S.C., et al. (2018). Gut microbiome modulates response to anti–PD-1 immunotherapy in melanoma patients. Science *359*, 97–103. https://doi.org/10.1126/science.aan4236.
5. Sepich-Poore, G.D., Zitvogel, L., Straussman, R., Hasty, J., Wargo, J.A., and Knight, R. (2021). The microbiome and human cancer. Science *371*, eabc4552. https://doi.org/10.1126/science.abc4552.
6. McKee, A.M., Kirkup, B.M., Madgwick, M., Fowler, W.J., Price, C.A., Dreger, S.A., Ansorge, R., Makin, K.A., Caim, S., Le Gall, G., et al. (2021). Antibiotic-induced disturbances of the gut microbiota result in accelerated breast tumor growth. iScience *24*, 103012. https://doi.org/10.1016/j.isci.2021.103012.
7. Kuczma, M.P., Ding, Z.-C., Li, T., Habtetsion, T., Chen, T., Hao, Z., Bryan, L., Singh, N., Kochenderfer, J.N., and Zhou, G. (2017). The impact of antibiotic usage on the efficacy of chemoimmunotherapy is contingent on the source of tumor-reactive T cells. Oncotarget *8*, 111931–111942. https://doi.org/10.18632/oncotarget.22953.
8. Routy, B., Le Chatelier, E., Derosa, L., Duong, C.P.M., Alou, M.T., Daillère, R., Fluckiger, A., Messaoudene, M., Rauber, C., Roberti, M.P., et al. (2018). Gut microbiome influences efficacy of PD-1–based immunotherapy against epithelial tumors. Science *359*, 91–97. https://doi.org/10.1126/science.aan3706.
9. Iida, N., Dzutsev, A., Stewart, C.A., Smith, L., Bouladoux, N., Weingarten, R.A., Molina, D.A., Salcedo, R., Back, T., Cramer, S., et al. (2013). Commensal Bacteria Control Cancer Response to Therapy by Modulating the Tumor Microenvironment. Science *342*, 967–970. https://doi.org/10.1126/science.1240527.
10. Vétizou, M., Pitt, J.M., Daillère, R., Lepage, P., Waldschmitt, N., Flament, C., Rusakiewicz, S., Routy, B., Roberti, M.P., Duong, C.P.M., et al. (2015). Anticancer immunotherapy by CTLA-4 blockade relies on the gut microbiota. Science *350*, 1079–1084. https://doi.org/10.1126/science.aad1329.
11. Sivan, A., Corrales, L., Hubert, N., Williams, J.B., Aquino-Michaels, K., Earley, Z.M., Benyamin, F.W., Lei, Y.M., Jabri, B., Alegre, M.-L., et al. (2015). Commensal Bifidobacterium promotes antitumor immunity and facilitates anti-PD-L1 efficacy. Science *350*, 1084–1089. https://doi.org/10.1126/science.aac4255.
12. Ivanov, I.I., and Honda, K. (2012). Intestinal Commensal Microbes as Immune Modulators. Cell Host Microbe *12*, 496–508. https://doi.org/10.1016/j.chom.2012.09.009.
13. Hooper, L.V., Littman, D.R., and Macpherson, A.J. (2012). Interactions Between the Microbiota and the Immune System. Science *336*, 1268–1273. https://doi.org/10.1126/science.1223490.
14. Viaud, S., Saccheri, F., Mignot, G., Yamazaki, T., Daillère, R., Hannani, D., Enot, D.P., Pfirschke, C., Engblom, C., Pittet, M.J., et al. (2013). The Intestinal Microbiota Modulates the Anticancer Immune Effects of Cyclophosphamide. Science *342*, 971–976. https://doi.org/10.1126/science.1240537.
15. Bessell, C.A., Isser, A., Havel, J.J., Lee, S., Bell, D.R., Hickey, J.W., Chaisawangwong, W., Glick Bieler, J., Srivastava, R., Kuo, F., et al. (2020). Commensal bacteria stimulate antitumor responses via T cell cross-reactivity. Jci Insight *5*, e135597. https://doi.org/10.1172/jci.insight.135597.
16. Tripodi, L., Passariello, M., D'Argenio, V., Leggiero, E., Vitale, M., Colicchio, R., Salvatore, P., Cerullo, V., and Pastore, C.D.L. (2021). Evaluation of the antiproliferative effect of Bifidobacterium longum BB-536 in solid tumor cell lines, co-cultured with murine splenocytes. Biochim. Clin. *45*, 242–247. https://doi.org/10.19186/bc_2021.021.
17. Capasso, C., Magarkar, A., Cervera-Carrascon, V., Fusciello, M., Feola, S., Muller, M., Garofalo, M., Kuryk, L., Tähtinen, S., Pastore, L., et al. (2017). A novel in silico framework to improve MHC-I epitopes and break the tolerance to melanoma.

OncoImmunology *6*, e1319028. https://doi.org/10.1080/2162402x.2017.1319028.

18. Nejman, D., Livyatan, I., Fuks, G., Gavert, N., Zwang, Y., Geller, L.T., Rotter-Maskowitz, A., Weiser, R., Mallel, G., Gigi, E., et al. (2020). The human tumor microbiome is composed of tumor type–specific intracellular bacteria. Science *368*, 973–980. https://doi.org/10.1126/science.aay9189.
19. Kalaora, S., Nagler, A., Nejman, D., Alon, M., Barbolin, C., Barnea, E., Ketelaars, S.L.C., Cheng, K., Vervier, K., Shental, N., et al. (2021). Identification of bacteria-derived HLA-bound peptides in melanoma. Nature *592*, 138–143. https://doi.org/10.1038/s41586-021-03368-8.
20. Zitvogel, L., Daillère, R., Roberti, M.P., Routy, B., and Kroemer, G. (2017). Anticancer effects of the microbiome and its products. Nat. Rev. Microbiol. *15*, 465–478. https://doi.org/10.1038/nrmicro.2017.44.
21. Feola, S., Capasso, C., Fusciello, M., Martins, B., Tähtinen, S., Medeot, M., Carpi, S., Frascaro, F., Ylosmäki, E., Peltonen, K., et al. (2018). Oncolytic vaccines increase the response to PD-L1 blockade in immunogenic and poorly immunogenic tumors. OncoImmunology *7*, e1457596. https://doi.org/10.1080/2162402x.2018.1457596.
22. Vitale, M., Scialò, F., Patriciello, T., Tripodi, L., Coluccino, L., Scognamiglio, A., and Pastore, L. (2023). Oncolytic adenovirus treatment induces the reduction of tumor dimension in a model of mice lung adenocarcinoma multicellular spheroids. Biochim. Clin. *47*, 251–258. https://doi.org/10.19186/bc_2023.045.
23. Vitale, M., Scialò, F., Passariello, M., Leggiero, E., D'Agostino, A., Tripodi, L., Gentile, L., Bianco, A., Castaldo, G., Cerullo, V., et al. (2022). Oncolytic Adenoviral Vector-Mediated Expression of an Anti-PD-L1-scFv Improves Anti-Tumoral Efficacy in a Melanoma Mouse Model. Front. Oncol. *12*, 902190. https://doi.org/10.3389/fonc.2022.902190.
24. Cerullo, V., Diaconu, I., Romano, V., Hirvinen, M., Ugolini, M., Escutenaire, S., Holm, S.-L., Kipar, A., Kanerva, A., and Hemminki, A. (2012). An Oncolytic Adenovirus Enhanced for Toll-like Receptor 9 Stimulation Increases Antitumor Immune Responses and Tumor Clearance. Mol. Ther. *20*, 2076–2086. https://doi.org/10.1038/mt.2012.137.
25. Garofalo, M., Bertinato, L., Staniszewska, M., Wieczorek, M., Salmaso, S., Schrom, S., Rinner, B., Pancer, K.W., and Kuryk, L. (2021). Combination Therapy of Novel Oncolytic Adenovirus with Anti-PD1 Resulted in Enhanced Anti-Cancer Effect in Syngeneic Immunocompetent Melanoma Mouse Model. Pharm. Times *13*, 547. https://doi.org/10.3390/pharmaceutics13040547.
26. Tripodi, L., Vitale, M., Cerullo, V., and Pastore, L. (2021). Oncolytic Adenoviruses for Cancer Therapy. Int. J. Mol. Sci. *22*, 2517. https://doi.org/10.3390/ijms22052517.
27. Hwang, J.K., Hong, J., and Yun, C.-O. (2020). Oncolytic Viruses and Immune Checkpoint Inhibitors: Preclinical Developments to Clinical Trials. Int. J. Mol. Sci. *21*, 8627. https://doi.org/10.3390/ijms21228627.
28. Chiaro, J., Kasanen, H.H.E., Whalley, T., Capasso, C., Grönholm, M., Feola, S., Peltonen, K., Hamdan, F., Hernberg, M., Mäkelä, S., et al. (2021). Viral Molecular Mimicry Influences the Antitumor Immune Response in Murine and Human Melanoma. Cancer Immunol. Res. *9*, 981–993. https://doi.org/10.1158/2326-6066.cir-20-0814.
29. Uribe-Herranz, M., Rafail, S., Beghi, S., Gil-de-Gómez, L., Verginadis, I., Bittinger, K., Pustylnikov, S., Pierini, S., Perales-Linares, R., Blair, I.A., et al. (2020). Gut microbiota modulate dendritic cell antigen presentation and radiotherapy-induced antitumor immune response. J. Clin. Invest. *130*, 466–479. https://doi.org/10.1172/jci124332.
30. Sasso, E., D'Avino, C., Passariello, M., D'Alise, A.M., Siciliano, D., Esposito, M.L., Froechlich, G., Cortese, R., Scarselli, E., Zambrano, N., et al. (2018). Massive parallel screening of phage libraries for the generation of repertoires of human immunomodulatory monoclonal antibodies. mAbs *10*, 1060–1072. https://doi.org/10.1080/19420862.2018.1496772.
31. Passariello, M., Camorani, S., Vetrei, C., Cerchia, L., and De Lorenzo, C. (2019). Novel Human Bispecific Aptamer–Antibody Conjugates for Efficient Cancer Cell Killing. Cancers *11*, 1268. https://doi.org/10.3390/cancers11091268.
32. Rastrelli, M., Tropea, S., Rossi, C.R., and Alaibac, M. (2014). Melanoma: epidemiology, risk factors, pathogenesis, diagnosis and classification. In Vivo *28*, 1005–1011.
33. Mellman, I., Coukos, G., and Dranoff, G. (2011). Cancer immunotherapy comes of age. Nature *480*, 480–489. https://doi.org/10.1038/nature10673.
34. Strati, F., Pujolassos, M., Burrello, C., Giuffrè, M.R., Lattanzi, G., Caprioli, F., Troisi, J., and Facciotti, F. (2021). Antibiotic-associated dysbiosis affects the ability of the gut microbiota to control intestinal inflammation upon fecal microbiota transplantation in experimental colitis models. Microbiome *9*, 39. https://doi.org/10.1186/s40168-020-00991-x.
35. Ericsson, A.C., and Franklin, C.L. (2015). Manipulating the Gut Microbiota: Methods and Challenges. ILAR J. *56*, 205–217. https://doi.org/10.1093/ilar/ilv021.
36. Matson, V., Fessler, J., Bao, R., Chongsuwat, T., Zha, Y., Alegre, M.-L., Luke, J.J., and Gajewski, T.F. (2018). The commensal microbiome is associated with anti–PD-1 efficacy in metastatic melanoma patients. Science *359*, 104–108. https://doi.org/10.1126/science.aao3290.
37. Ley, R.E., Turnbaugh, P.J., Klein, S., and Gordon, J.I. (2006). Human gut microbes associated with obesity. Nature *444*, 1022–1023. https://doi.org/10.1038/4441022a.
38. Rawls, J.F., Mahowald, M.A., Ley, R.E., and Gordon, J.I. (2006). Reciprocal Gut Microbiota Transplants from Zebrafish and Mice to Germ-free Recipients Reveal Host Habitat Selection. Cell *127*, 423–433. https://doi.org/10.1016/j.cell.2006.08.043.
39. Jandhyala, S.M., Talukdar, R., Subramanyam, C., Vuyyuru, H., Sasikala, M., and Nageshwar Reddy, D. (2015). Role of the normal gut microbiota. World J. Gastroentero. *21*, 8787–8803. https://doi.org/10.3748/wjg.v21.i29.8787.
40. Callahan, B.J., McMurdie, P.J., Rosen, M.J., Han, A.W., Johnson, A.J.A., and Holmes, S.P. (2016). DADA2: High-resolution sample inference from Illumina amplicon data. Nat. Methods *13*, 581–583. https://doi.org/10.1038/nmeth.3869.
41. McMurdie, P.J., and Holmes, S. (2013). phyloseq: An R Package for Reproducible Interactive Analysis and Graphics of Microbiome Census Data. PLoS One *8*, e61217. https://doi.org/10.1371/journal.pone.0061217.
42. Wright, E. (2016). Using DECIPHER v2.0 to Analyze Big Biological Sequence Data in R. R. J. *8*, 352. https://doi.org/10.32614/RJ-2016-025.
43. Schliep, K.P. (2011). phangorn: phylogenetic analysis in R. Bioinformatics *27*, 592–593. https://doi.org/10.1093/bioinformatics/btq706.
44. Dunn, O.J. (1964). Multiple Comparisons Using Rank Sums. Technometrics *6*, 241–252. https://doi.org/10.2307/1266041.
45. Caron, E., Espona, L., Kowalewski, D.J., Schuster, H., Ternette, N., Alpízar, A., Schittenhelm, R.B., Ramarathinam, S.H., Lindestam Arlehamn, C.S., Chiek Koh, C., et al. (2015). An open-source computational and data resource to analyze digital maps of immunopeptidomes. Elife *4*, e07661. https://doi.org/10.7554/elife.07661.
46. Kilkenny, C., Browne, W.J., Cuthill, I.C., Emerson, M., and Altman, D.G. (2010). Improving Bioscience Research Reporting: The ARRIVE Guidelines for Reporting Animal Research. PLoS Biol. *8*, e1000412. https://doi.org/10.1371/journal.pbio.1000412.
47. Iaffaldano, L., Granata, I., Pagliuca, C., Esposito, M.V., Casaburi, G., Salerno, G., Colicchio, R., Piccirillo, M., Ciacci, C., Del Vecchio Blanco, G., et al. (2018). Oropharyngeal microbiome evaluation highlights Neisseria abundance in active celiac patients. Sci. Rep. *8*, 11047. https://doi.org/10.1038/s41598-018-29443-1.
48. Nardelli, C., Granata, I., D'Argenio, V., Tramontano, S., Compare, D., Guarracino, M.R., Nardone, G., Pilone, V., and Sacchetti, L. (2020). Characterization of the Duodenal Mucosal Microbiome in Obese Adult Subjects by 16S rRNA Sequencing. Microorg *8*, 485. https://doi.org/10.3390/microorganisms8040485.
49. Hollander, M., Wolfe, D.A., and Chicken, E. (2017). Nonparametric Statistical Methods: Hollander/Nonparametric Statistical Methods. https://doi.org/10.1002/9781119196037.
50. Tripodi, L., Sasso, E., Feola, S., Coluccino, L., Vitale, M., Leoni, G., Szomolay, B., Pastore, L., and Cerullo, V. (2023). Systems Biology Approaches for the Improvement of Oncolytic Virus-Based Immunotherapies. Cancers *15*, 1297. https://doi.org/10.3390/cancers15041297.
51. Andreatta, M., and Nielsen, M. (2016). Gapped sequence alignment using artificial neural networks: application to the MHC class I system. Bioinformatics *32*, 511–517. https://doi.org/10.1093/bioinformatics/btv639.

STAR★METHODS

KEY RESOURCES TABLE

REAGENT or RESOURCE	SOURCE	IDENTIFIER
Antibodies		
anti-mouse CD3 PerCP-Cy5.5	eBioscience, Invitrogen	Cat# 45-0031-82; RRID: AB_1107000
anti-mouse CD8 FITC	eBioscience, Invitrogen	Cat# 11-0083-82; RRID: AB_657764
anti-mouse CD4 PeCy7	eBioscience, Invitrogen	Cat# 25-0041-82; RRID: AB_469576
anti-mouse CD45R/B220 APC	Biolegend, San Diego, California	Cat# 103211; RRID: AB_312996
anti-mouse CD45 APC-Cy7	Sony Biotechnology, San Jose, California	Cat# 1153580; RRID: N/A
anti-mouse IFN-γ PE	Biolegend, San Diego, California	Cat# 505807; RRID: AB_315401
anti-mouse Foxp3 PE	eBioscience, Invitrogen	Cat# 12-5773-82; RRID: AB_465936
FC-Block	Biolegend, San Diego, California	Cat# 101301; RRID: AB_312800
Bacterial and virus strains		
Ad5D24-CpG	Prof.Vincenzo Cerullo	Cerullo et al.[24]
Chemicals, peptides, and recombinant proteins		
Cell stimulation cocktail	eBioscience, Invitrogen	Cat# 00-4970-03
Brefeldin A	eBioscience, Invitrogen	Cat# 00-4506-51
Foxp3/Transcription Factor Staining Buffer Set	eBioscience, Invitrogen	Cat# 00-5523-00
Critical commercial assays		
CyQUANT™LDH Cytotoxicity Assay	Invitrogen	Cat# C20300
Mouse IFN-γ 96-well White Precoated	Immunospot, CTL Europe GmbH	Cat# SKU: hIFNgp-1M
QIAamp DNA mini kit	Qiagen, Venlo, The Netherlands	Cat# 56304
Agencourt AMPure XT beads	Beckman Coulter, Brea, CA, USA	Cat# A63881
Deposited data		
Sample metadata and raw data Release data: 2023-10-31	NCBI Sequence Read Archive (SRA) https://www.ncbi.nlm.nih.gov/sra/PRJNA999658	BioProject accession number PRJNA999658
Experimental models: Cell lines		
B16.OVA	Prof. Vincenzo Cerullo	Sigma-Aldrich Cat# SCC420
Experimental models: Organisms/strains		
Female C57BL/6J 6–8 weeks old	Charles Rivers Italy RMS	Cat# 632C57BL/6J
Authorization number by the Ministry of Health	Provincial Government of Italy	n°331/2019-PR-protocol D5A89.35
Software and algorithms		
DADA2 v. 1.15.0	Callahan et al.[40]	(https://github.com/benjjneb/dada2
Phyloseq 1.28.0 R packages	McMurdie et al.[41]	R version 3.6.1
SILVA reference database v.128	https://zenodo.org/record/824551#.XmIcO5NKhuU	N/A
DECIPHER 2.12.0 R package	Wright et al.[42]	N/A
phangorn 2.5.5 R package	Schliep et al.[43]	N/A
FSA 0.8.27 package	Dunn et al.[44]	N/A
909 H-2Kb-specific peptides from B16-F10 murine melanoma cell line	Caron et al.[45]	ProteomeXchange (Accession no: PXD001872)
Microbial peptides database	NCBI protein databases	https://www.ncbi.nlm.nih.gov/protein/
in silico tool Homology Evaluation Xenopeptides (HEX)	Chiaro et al.[28]	https://whalleyt.shinyapps.io/homology-evalutation-xenopeptides/.

(*Continued on next page*)

Continued

REAGENT or RESOURCE	SOURCE	IDENTIFIER
NetMHC		
GraphPad Prism 7 software	GraphPad Software, Inc., La Jolla, CA, USA	D4106509D18
Other		
Standard diet mice	Diete standard	Cat# 4RF25
Vancomycin	Mylan	Cat# MINSAN 041220070
ProBiotaTM Bifido Seeking health 10 Billion Bifidobacterium	Sivan et al.[11]	Probiotic Blend (10 billion CFU) in a 280 mg* base of inulin (derived from chicory root)

RESOURCE AVAILABILITY

Lead contact

Further information and requests for resources and reagents should be directed to and will be fulfilled by the lead contact, Lucio Pastore (lucio.pastore@unina.it)

Materials availability

This study did not generate new unique reagents.

Data and code availability

- The datasets used and/or analyzed during the current study is publicly accessible. Information specific to these datasets are listed in the key resources table.
- Sample metadata and raw data obtained from 16S bacterial rRNA sequencing of fecal samples from mice enrolled in the experiment *in vivo* are reported in NCBI Sequence Read Archive (SRA), the BioProject accession number is PRJNA999658.
- This paper does not report original code. Any additional information required to reanalyze the data reported in this paper is available from the lead contact upon request.

EXPERIMENTAL MODEL AND STUDY PARTECIPANT DETAILS

Animal experiments

All animal experiments were reviewed and approved by the body responsible for animal welfare (OPBA) and by experimental animal committee of the CEINGE Biotecnologie Avanzate Franco Salvatore and the Provincial Government of Italy (n°331/2019-PR-protocol D5A89.35) national regulations guidelines in accordance with EU Directive 2010/63/EU. We used the ARRIVE 1 reporting guidelines.[46] Female C57BL/6J 6–8 weeks old were obtained from Charles Rivers and used as syngeneic mouse melanoma model. Animals were kept in individually ventilated cages under standard conditions (12 h light:dark, temperature-controlled and humidity-controlled conditions) and received *ad libitum* access to water and food. Animals were fed with diet standard (Mucedola) and housed in Animal Biosafety Level 2 (ABSL-2) in an animal facility at CEINGE Biotecnologie Avanzate Franco Salvatore. Drinking water was sterilized in an autoclave and changed every two days. Animals were monitored daily for symptoms related to distress and pain including hunched posture, overall activity/ability to move and roughness of the hair coat. 3.5×10^5 B16.OVA cells were engrafted subcutaneously in right flank of all animals. After 7–9 days from inoculation, we ensured that all the tumors were implanted and have reached a diameter of 5 mm and then were randomized into treated and control groups. Blinding from the people running the study and analysing the data was adopted during some stages of animal experiments: during animal's allocation to a group, the conduct of the experiment and during the outcome assessment. Some animals have been dropped from the study and euthanized before the endpoint, when the size of the largest diameter of the subcutaneous tumor exceeded 18 mm. To guarantee a sample-size for each experimental group equal to 5 and 6 animals useful for statistical analyses, as described in figure legends, experimental units in each group at the start of the study were respectively equal to 7 and 8 animals. Animal experiments were not replicated. In the present study, we collected spleen and tumor samples for flow cytometry analyses and feces samples from all enrolled animals in experimental research of treatment with Bifidus and Ad-CpG. Spleen and tumor samples were triturated into single-cell suspension in a sterile freezing medium with 90% FBS and 10% DMSO, then filtered by a cell strainer 70 μm and stored at −80°C. Viable cells were counted using an automated cell counter. Feces samples were immediately cooled in dry ice and stored at −80°C until DNA extraction for microbiome analysis. For the preimmunization experiment, 5-6 weeks-old female C57BL/6J (n = 3 per group) were allocated in different groups according to the treatment and each mouse was subcutaneously injected with 25 μg of Bifidobacterium peptide complexed with 25 μg of poly (I:C) adjuvant. The prime and boosting were done respectively on days 0 and 7 and mice were sacrificed on day 14.

Tumor implantation and tumor growth measurement

At day 0, 3.5 × 10^5 B16.OVA cells were diluted in 200 μL of PBS and injected subcutaneously into the right flank of each mouse. 9 days after cell inoculation, tumors were measured with an electronic digital caliper (largest tumor diameter and perpendicular tumor diameter) every two days, starting on the day cancer cell inoculation. Tumors volume was calculated as length × width × height (mm^3). Mice were sacrificed when the tumor volume was greater than 1.800 mm^3 or when they were in poor condition and expected to die shortly. Tumors and spleens were collected and used for further experiments. In the *In vivo* experiment related to restoring Ad-CpG efficacy in vancomycin-treated mice (Figure 2, panel E), the survival of treated mice has been followed until they were sacrificed or naturally died. Additional specific details of each animal experiment are well described in figure legends and by experimental design representations.

Virus administration

Mice were anesthetized in an isoflurane chamber and then 1 × 10E9 vp of Ad-CpG was injected intratumorally at days 9, 11 and 13 after cell inoculation. The protocol schedule of tumor, Ad-CpG injection is shown in Figure 1, panel A.

Antibiotic and *bifidobacterium* treatment

Mice were treated with vancomycin starting two weeks before tumor cells inoculation until the first injection of Ad-CpG. Vancomycin (0.25 mg/mL Mylan) was administered by oral gavage every two days. A cocktail of lyophilized *Bifidobacterium* spp. (*B. bifidum, B. longum, B. lactis* and *B. breve*- Seeking Health) was resuspended in PBS at a 5 × 10E9 CFU/mL concentration. Each mouse was treated with 200 μL of *Bifidobacterium* spp. (1 × 10E9 CFU/mouse) added to the drinking water starting 15 days before tumor inoculation and until the end of the experiment.

METHOD DETAILS

Cell lines and reagents

B16.OVA, a mouse melanoma cell line expressing chicken ovalbumin (OVA) derived from C57BL/6J, was kindly provided by Prof. Vincenzo Cerullo. Cells were cultured according to ATCC recommendations in RPMI 1640 medium. Medium was supplemented with 10% heat-inactivated fetal bovine serum (FBS, Gibco), penicillin (50 U/mL), streptomycin (500 μg/mL), and glutamine (4 mmol/L) in a humidified atmosphere with 5% CO_2 at 37°C. 1% of Geneticine (GIBCO) was added to the cells. At the endpoint of *in vivo* experiments, peripheral blood mononuclear cells (PBMCs) were isolated from the spleens of treated mice, to perform the IFN-γ ELISpot.

Virus production

Oncolytic adenovirus Ad5D24-CpG was amplified and characterized using standard protocols, as previously described.[24] For a first step of amplification, A549 cells infected with virus Ad5D24-CpG at MOI (multiplicity of infection) equal to 10 pfu/cell. After 72h, the cell lysate was collected and stored at −80°C. Subsequently, to induce cell lysis, the sample was subjected to three freeze-thaw cycles and then centrifuged at 4,000 rpm for 25 min at 25°C. The supernatant containing the virus was collected and purified from the lysate by a first step in an ultracentrifuge at 27,000 rpm for 1-2h at 4°C on a cesium chloride (CsCl) gradient. The band containing the oncolytic adenovirus was subjected to a further ultracentrifugation step under the same conditions described above for a time exceeding 18h. Successively, the sample was dialyzed by placing it in TM solution (10 mM Tris-HCl pH 8.0, 2 mM MgCl2) for 2h under stirring at 4°C. After 2h, the dialysis cassette was transferred to the Freezing solution (10 mM Tris-HCl pH 8.0, 2 mM MgCl2, 4% sucrose) overnight at 4°C under stirring. The virus was collected, aliquoted and stored at −80°C. Ad5D24-CpG was titrated by spectrophotometric reading, obtaining a titer of 4.4 × 10E11 vp/mL.

Tumor cell lysis assays

Tumor cell lysis was determined through the quantitative analysis of Lactate dehydrogenase (LDH) by using an LDH Detection Kit (Cyquant, Invitrogen), according to the manufacturer's instructions. The B16-OVA were plated and incubated for 16 h at 37°C, and successively pre-immunized murine splenocytes were added at ratio of 5:1. After 48 h of incubation at 37°C, images of each experimental point, before and after the removal of the murine splenocytes were captured by a phase-contrast microscopy. The dosage of LDH activity was performed on the supernatants collected 48-h of co-culture assay, by spectrophotometric analysis at 490 nm.

Isolation of immune cells from mice spleen and tumor

After the collection, spleen and tumor samples were kept in sterile RPMI 1640 medium, supplemented with 10% heat-inactivated fetal bovine serum (FBS, Gibco), and transferred into a 70 μm cell strainer fitted on a 50 mL tube. Then spleen and tumor samples were gently cut into small pieces using a 5 mL syringe plunger and pressed through a cell strainer. Once the single-cell suspensions were collected, up to 25–30 mL of media was added and cells were centrifuged at 2,000 rpm, 10 min, at +4°C. Splenocytes and tumor cells were centrifuged at 2,000 rpm, 10 min, at +4°C and filtered through a new 70 μm cell strainer, to remove dead cell clumps and other debris. Some cells were used directly for cell assays and IFN-γ ELISpot while the remaining cells were frozen in a medium supplemented with 90% of FBS and 10% of DMSO.

Flow cytometry analysis

Surface and intracellular staining were performed using the following anti-mouse antibodies: CD3 PerCP-Cy5.5 (eBioscience, Invitrogen); CD8 FITC (eBioscience, Invitrogen); CD4 PeCy7 (eBioscience, Invitrogen); CD45R/B220 APC (Biolegend, San Diego, California); CD45 APC-Cy7 (Sony Biotechnology, San Jose, California); IFN-γ PE (Sony Biotechnology); Foxp3 PE (eBioscience, Invitrogen). Cell stimulation cocktail (eBioscience, Invitrogen); Brefeldin A (eBioscience, Invitrogen). Cells were initially stained with surface markers (CD3, CD8, CD4, CD45R/B220 and CD45) and then stained for Foxp3 (Foxp3/Transcription Factor Staining Buffer Set, eBioscience, Invitrogen) using a protocol for nuclear detection, according to manufacturers' instructions. T-cells were stimulated to produce IFN-γ *in vitro* using a cell stimulation cocktail (eBioscience, Invitrogen) and its secretion was blocked using protein transport inhibitors (Brefeldin A Solution) (eBioscience, Invitrogen). Subsequently, cells were stained with surface markers (CD3, CD8, CD4, CD45R/B220 and CD45) and then stained for IFN-γ using a protocol for cytoplasmatic detection, according to manufacturers' instructions. All stained cells were acquired by FACS Canto II cytometer (BD Biosciences Franklin Lakes, NJ) and analyzed with FACS Diva software (BD Biosciences).

IFN-γ ELISpot

IFN-γ ELISpot assays were performed using a commercially available mouse ELISpot reagent set (Mouse IFN-γ 96-well White Precoated, ImmunoSpot, Bonn Germany) and 0.02 μg/μL of each peptide was tested *in vitro* stimulations of 3×10^5 splenocytes for each well at 37°C for 72h. The experiments were performed in duplicate in each 96-well. Spots were counted using an ELISpot reader system (ImmunoSpot, Bonn Germany).

Graphics

The graphical representations, schematics, and timelines used in the figures were created using BioRender.com.

QUANTIFICATION AND STATISTICAL ANALYSIS

16S rRNA microbiome sequencing

Five fecal samples were collected from every group (n = 5) at different time points: before B16.OVA cells inoculation (day-10), when tumor has reached a diameter of 5 mm and before treatment (day 0), the day before the last feeding integration with the *Bifidobacterium* spp. mix (day 18), and at the end of the experiment (day 20) as described in the related paragraph. DNA was extracted from fecal samples using a QIAamp DNA mini kit (Qiagen, Venlo, The Netherlands). All extractions were performed in a pre-PCR designated room. To deeply investigate microbiome composition, we used a multiplexed 16S rDNA amplicon-based approach coupled with the NGS system MiSeq (Illumina, San Diego, CA, USA).[47,48] In particular, 500 bp amplicons, spanning the V4-V6 hyper-variable regions of the 16S rRNA gene, were obtained. Each sample was individually amplified and purified (Agencourt AMPure XT beads, Beckman Coulter, Brea, CA, USA). Primers used in the first round of PCR contained the overhang sequences with Illumina adapters:

forward primer, 5′- TCGTCGGCAGCGTCAGATGTGTATAAGAGACAGCCAGCAGCCGCGGTAA -3′; reverse primer, 5′- GTCTCGTGGGCTCGGAGATGTGTATAAGAGACAGGGGTTGCGCTCGTTGC - 3′. PCR conditions were 95°C for 10 min; 30 cycles of 95°C for 30 s, 59°C for 30 s, 72°C for 1 min; 72°C for 7 min and 4°C to the end. A second round of PCR was used to add the Illumina index to the amplicons for the library preparation according to the Nextera XT protocol (Illumina). PCR conditions were 72°C for 3 min; 95°C for 30 s; 12 cycles of 95°C for 10 s, 55°C for 30 s, and 72°C for 30 s; 72°C for 5 min and 10°C to the end. After appropriate quality assessment (TapeStation, Agilent Technologies, Santa Clara, CA, USA), the amplification products from different DNA samples were pooled in equimolar ratios. The obtained multiple amplicon libraries were quality assessed (TapeStation, Agilent Technologies) and quantified (Qubit dsDNA BR assay, Thermo Fisher, Waltham, MA, USA), according to the manufacturer's instructions, in order to obtain a pool of equimolar libraries, so ensuring a normalization across the different samples sequenced in the same run. All libraries were sequenced with the Illumina MiSeq System, PE 300 × 2 protocol, according to the specifications of the manufacturer.

Microbiome data processing

Quality of microbial sequences was assessed using MultiQC v1.5 [1]. Reads adapters and low-quality reads/ends were removed using Trimmomatic v0.38. To analyze the taxonomic composition of samples, DADA2 v. 1.15.0[40] and Phyloseq 1.28.0[41] R packages were used (R version 3.6.1). As a scarce overlapping between paired-end reads was observed, we chose to analyze only the forward reads to have a more reliable alignment. Before aligning reads, the forward primer was trimmed out from reads and reads were filtered according to the following parameters: maxEE = 2; minLen = 50; maxN = 0; truncQ = 2. After chimeric sequences removal, taxonomy was assigned to ASVs (Amplicon Sequence Variants) by using the SILVA reference database v.128, formatted for being used by DADA2 software and available at the link https://zenodo.org/record/824551#.XmIcO5NKhuU. The phylogenetic tree was constructed by performing a multiple-alignment using the DECIPHER 2.12.0 R package.[42] The phangorn 2.5.5 R package[43] was then used to first construct a neighbor-joining tree, and then fit a GTR+-G+I (Generalized time-reversible with Gamma rate variation) maximum likelihood tree using the neighbor-joining tree as a starting point. Statistical analyses of the dataset were carried out through combining all the data (cleaned ASVs, taxa assignment, phylogenetic tree, and metadata) into a phyloseq object. The α- and β-diversity were computed on the counts normalized with the respect to the total and the ANOSIM tests were performed. Wilcoxon rank-sum test (Mann-Whitney) was applied to test significance in terms of richness measured by the several α-diversity distances. The significance of differential abundance among groups at different taxonomic levels was assessed by

the Kruskal-Wallis Rank-Sum Test in R environment.[49] The pairwise comparison was then performed by Dunn's test[44] (FSA 0.8.27 package) on the significant Kruskal-Wallis tests and the p value corrected for multiple comparisons by the Benjamini-Hochberg adjustment.

Discovery and characterization of microbial peptides

We collected 909 H-2Kb-specific peptides from B16-F10 murine melanoma cell line obtained from Caron et al.[45] These 909 murine peptides were used to search microbial peptides from *Bifidobacterium bifidum, Bifidobacterium longum, Bifidobacterium breve and Bifidobacterium lactis* NCBI protein databases (https://www.ncbi.nlm.nih.gov/protein/) based on Hamming similarity measure. We identified 62 unique pairs of melanoma-microbial peptides (58 pairs with Hamming distance 1 and 4 pairs with Hamming distance 3). These were analyzed using the *in silico* tool Homology Evaluation Xenopeptides (HEX), published in[28,50] and available at https://whalleyt.shinyapps.io/homology-evalutation-xenopeptides/. HEX compares the similarity between melanoma peptides (reference peptides) and microbial peptides (query peptides) by calculating the weighted alignment score, using the BLOSUM substitution matrix, and predicting the H-2Kb binding affinity, using NetMHC.[51]

Fourteen unique murine-microbial peptide pairs (comprising fourteen B16.F10 peptides and ten microbial peptides) were selected based on their alignment and binding affinity scores (Table 1) for *in vivo* and *in vitro* experiments. The schematic of the bioinformatics workflow is shown in Figure 6, panel A. All peptides identified and tested *in vitro* and *in vivo* were purchased from Twin Helix. 14mg of each peptide was ordered with a guaranteed purity of >90%. The immunogenic peptides tested are reported in Table 1.

Statistical analysis

Statistical analyses were performed using the GraphPad Prism 7 software (GraphPad Software, Inc., La Jolla, CA, USA). Data were represented as mean +/− standard error of the mean (SEM) or +/−standard deviation (SD) as well defined in the figure legends. Significant differences of tumor growth between different groups was analyzed by two-way analysis of variance (ANOVA), and a p value <0.05 was considered statistically significant for all test used (*$p < 0.05$, **$p < 0.005$, ***$p < 0.001$, ****$p < 0.0001$). For average area under the curves (AUC) relative to tumor growth in the different experimental groups indicated as mean ± SEM, the statistical significance was evaluated by Unpaired T-test with Welch's correction. The log rank Mantel-Cox analysis was used to calculate the p value ($p < 0.05$) of the survival curves. The statistical significance of percentages of T lymphocytes between experimental groups was evaluated by two-way ANOVA test using Tukey's multiple comparison test. The statistical significance of percentages of IFN-γ+ T-cells between groups was evaluated by paired student's T-test. The relative abundances of differentially abundant genera ($p < 0.05$) among the four-time points for each treatment was evaluated according to the Kruskal-Wallis test. Regarding the significance of distribution differences, between the three genera with a relative abundance >2%, has been calculated by applying the Kruskal-Wallis test, Dunn's post-hoc test and Benjamini-Hochberg p value adjustment. Comparison between levels of immunogenicity between Bifidobacterium-derived peptides, the statistical analysis was performed by ordinary one-way ANOVA test. Further details about the statistical tests for each experiment can be found in the corresponding figure legends.